

Extensive study of phase diagram for charge neutral homogeneous quark matter affected by dynamical chiral condensation

– unified picture for thermal unpairing transitions from weak to strong coupling –

Hiroaki Abuki^{1,*} and Teiji Kunihiro^{1,†}

¹ Yukawa Institute for Theoretical Physics, Kyoto University, Kyoto 606-8502, Japan

(Dated: December 23, 2019)

We study the phase structures of charge neutral quark matter under the β -equilibrium for a wide range of the quark-quark coupling strength within a four-Fermion model. A comprehensive and unified picture for the phase transitions from weak to strong coupling is presented. We first develop a technique to deal with the gap equation and neutrality constraints without recourse to numerical derivatives, and show that the off-diagonal color densities automatically vanish with the standard assumption for the diquark condensates. The following are shown by the numerical analyses: (i) The thermally-robustest pairing phase is the two-flavor pairing (2SC) in any coupling case, while the second one for relatively low density is the up-quark pairing (uSC) phase or the color-flavor locked (CFL) phase depending on the coupling strength and the value of strange quark mass. (ii) If the diquark coupling strength is large enough, the phase diagram is much simplified and is free from the instability problems associated with imaginary Meissner masses in the gapless phases. (iii) The interplay between the chiral and diquark dynamics may bring a non-trivial first order transition even in the pairing phases at high density. We confirm (i) also by using the Ginzburg-Landau analysis expanding the pair susceptibilities up to quartic order in the strange quark mass. We obtain the analytic expression for the doubly critical density where the two lines for the second order phase transitions merge, and below which the down-quark pairing (dSC) phase is taken over by the uSC phase. Also we study how the phase transitions from fully gapped states to partially ungapped states are smeared at finite temperature by introducing the order parameters for these transitions.

PACS numbers: 12.38.-t, 25.75.Nq

I. INTRODUCTION

Surprisingly rich phase structure of quark matter is being revealed by extensive theoretical studies [1–3]. On the basis of the asymptotic-free nature of QCD and the attraction between quarks due to a gluon exchange, it is now believed that the ground state of the sufficiently cold and extremely dense matter is in the color-flavor locked (CFL) phase where all the quark species equally participate in pairing [4]. In contrast, it remains still controversial what phase sets in next to the CFL as the density is decreased and/or the temperature is raised.

At zero temperature ($T = 0$), the following two ingredients play crucial roles for determining the second densest phase in QCD; (i) the strange quark mass [5–7], and (ii) the charge neutrality constraints as well as the β -equilibrium condition [8–10]. The former tends to bring a Fermi-momentum mismatch between the light and strange quarks, while the latter in the paired phase tends to match the Fermi-momenta by tuning the charge chemical potentials. Some theoretical studies suggest that, when the baryon density is decreased, the effect (ii) in the CFL phase cancels the effect (i) down to some critical density, at which the CFL phase turns into the gapless CFL (gCFL) phase [11]. In the realistic quark

matter in compact stars, the effect of (ii) gives so strong constraint because of a long range nature of gauge interactions that such an exotic phase may exist stably. The gCFL phase has been extensively studied and claimed to be the most promising candidate of next phase down in density at vanishing temperature [11] and is also known to lead an interesting astrophysical consequence on the cooling history of an aged compact star [12]. It should be, however, noted here that the gapless phases are usually accompanied by some transverse gluonic modes with imaginary Meissner mass at low temperature [13, 14], indicating the existence of more stable exotic states [15–21]. Although the resolution of the instability or finding the possible new stable state is now one of the central issues in this field, we won’t deal with this problem; nevertheless we will give some suggestions to possible resolution on the basis of the results obtained in this work.

The neutrality constraints are also known to bring about an interesting phase even at finite temperature ($T \neq 0$). In fact, a Ginzburg-Landau analysis shows that the d quark pairing phase with the $u-d$ and $d-s$ pairings, denoted by “dSC”, appears as the second phase when the 2SC (CFL) phase is cooled (heated) [22]. The existence of such a kind of intermediate phase has also been confirmed using the NJL model [23]. Also the gapless version of the dSC with an additional gapless mode is also examined for finite temperature [22] and for zero temperature [24]; the gapless dSC is shown to be always a metastable at zero temperature, while it may exist stably for nonzero temperature. It should be noted, however, that the gap-

*E-mail: abuki@yukawa.kyoto-u.ac.jp

†E-mail: kunihiro@yukawa.kyoto-u.ac.jp

less phase for nonzero temperature cannot be thermodynamically distinguished from the fully gapped one; in fact, it has no distinct phase boundary with the gapped one, and thus is of less physical interest than that at zero temperature.

In the most of the literature concerning the pairing phases of the quark matter [11, 23, 25], the strange quark mass is treated as a parameter just like an external magnetic field applied to a metallic superconductor [26]. In QCD, however, the strong attraction exists in the scalar quark-antiquark channel which leads to a non-perturbative phenomenon called the dynamical chiral condensation in the low density regime. It is interesting to investigate how the incorporation of the dynamical formation of the chiral condensates affects color superconducting phases [27, 28]. The competition between the chiral and diquark condensations under the charge neutrality constraints was first investigated in a four-Fermion model [24]; it was shown that the second densest phase next to the CFL strongly depends on the quark-quark (diquark) coupling strength, and in particular, the gapless CFL phase may be washed out from the phase diagram except for an extremely weak coupling case. Their investigation is extended to finite temperatures [29, 30] and recently also applied to the system with finite neutrino density [31]. Some of the results obtained in [29, 30], however, seemingly contradict with the previous claim by the authors of [22, 23] on the appearance of the dSC phase. This is one of puzzles indicating that a further investigation is needed for a systematic understanding of the phases of quark matter and transitions among them.

A main aim of this paper is to explore the phase diagram for a wide range of diquark coupling systematically and thereby give a unified picture for the phase transitions from weak to strong coupling. We clarify the detailed mechanism and features of thermal phase transitions, and make clear the relations among the previous studies [22, 23, 29, 30]. In particular, we shall study the the following. (i) How the (μ, T) -domain accommodating the pairing grows and that for the gapless phases vanishes as the coupling in the scalar diquark channel is increased. (ii) How we can draw a unified picture for the thermal unpairing phase transitions from weak to strong coupling; for this purpose, we extend the previous study [22] by making re-analysis of Ginzburg-Landau expansion focusing on the effects of the terms quartic in the strange quark mass. (iii) How and why non-trivial first order phase transitions could be caused by the competition between the pairing and chiral dynamics in the strange quark sector. (iv) How the transition from the fully gapped phase to the partially ungapped (gapless) one is smeared at finite temperature by introducing a definite order parameter.

The paper is organized as follows. In Sec. II, we introduce the model and derive the gap equation under the neutrality constraints. Some technical developments are presented, by which the numerical derivatives can be

replaced by simple algebraic equations. In Sec. III, we discuss the points listed above based on the numerical results. Also the Ginzburg-Landau analysis is performed and some interesting aspects of the thermal phase transitions are given at the end of this section. The summary and outlook are provided in Sec. IV. In Appendix A, we derive the Ginzburg-Landau potential expanded up to quartic order in the strange quark mass. In Appendix B, we show that the off-diagonal color densities automatically vanish under the standard ansatz for the diquark condensates.

II. FORMULATION

In this section, we introduce our model and formulate the mean field approximation under the kinetic constraints. In Sec. II B, we present some useful algebraic techniques to solve the gap equation and constraints without recourse to numerical derivatives.

A. Model

We start with the following Lagrangian as in [24]

$$\mathcal{L} = \bar{q}(i\partial - \mathbf{m}_0 + \boldsymbol{\mu}\gamma_0)q + \frac{G_d}{16} \sum_{\eta=1}^3 [(\bar{q}P_\eta^t\bar{q})(^tq\bar{P}_\eta q)] + \frac{G_s}{8N_c} [(\bar{q}\boldsymbol{\lambda}_F q)^2 + (\bar{q}i\gamma_5\boldsymbol{\lambda}_F q)^2]. \quad (1)$$

Here, $\boldsymbol{\lambda}_F = \{\sqrt{2/3}\mathbf{1}, \vec{\lambda}_F\}$ are the unit matrix and the Gell-Mann matrices in the flavor space. P_η is defined as [11]

$$(P_\eta)_{ij}^{ab} = i\gamma_5 C \epsilon^{\eta ab} \epsilon_{\eta ij} \quad \text{no sum over index } \eta \quad (2)$$

and $\bar{P}_\eta = \gamma_0(P_\eta)^\dagger \gamma_0$. a, b, \dots and i, j, \dots represent the color and flavor indices, respectively. The second term in Eq. (1) simulates the attractive interaction in the color anti-triplet, flavor anti-triplet and $J^P = 0^+$ channel in QCD. $\mathbf{m}_0 = \text{diag.}\{m_u, m_d, m_s\}$ is the current-quark mass matrix. In order to impose the color and electric neutralities, we have introduced in Eq. (1) the chemical potential matrix $\boldsymbol{\mu}$ in the color-flavor space as

$$\begin{aligned} \boldsymbol{\mu}_{ij}^{ab} = & \mu - \mu_e Q_{ij} + \mu_3 T_3^{ab} + \mu_8 T_8^{ab} \\ & + \mu_1 T_1^{ab} + \mu_2 T_2^{ab} + \mu_4 T_4^{ab} \\ & + \mu_5 T_5^{ab} + \mu_6 T_6^{ab} + \mu_7 T_7^{ab}. \end{aligned} \quad (3)$$

$Q = \text{diag.}(2/3, -1/3, -1/3)$ counts electric charge of each quark species. $T_3 = \text{diag.}(1/2, -1/2, 0)$ and $T_8 = \text{diag.}(1/3, 1/3, -2/3)$ are the diagonal charges for quarks in the fundamental representation of the color SU(3). We

have included the second and third lines in Eq. (3) which stand for the chemical potentials for off-diagonal color charges: It has been recently claimed that these chemical potentials should be included for the complete color neutralities [32]. We can prove, however, that if the diquark condensates have the color-flavor structure as given by Eq. (2), then the off-diagonal color densities must automatically vanish for $\mu_1 = \mu_2 = \mu_4 = \mu_5 = \mu_6 = \mu_7 = 0$; see Appendix B for the detail of the proof. Thus, we can safely adopt the usual diagonal ansatz for the chemical potential matrix. The explicit forms of the diagonal elements ($\mu_{ai} = \mu_{ii}^{aa}$) are as follows.

$$\begin{aligned}
\mu_{ru} &= \mu - \frac{2}{3}\mu_e + \frac{1}{2}\mu_3 + \frac{1}{3}\mu_8, \\
\mu_{gd} &= \mu + \frac{1}{3}\mu_e - \frac{1}{2}\mu_3 + \frac{1}{3}\mu_8, \\
\mu_{bs} &= \mu + \frac{1}{3}\mu_e - \frac{2}{3}\mu_8, \\
\mu_{rd} &= \mu + \frac{1}{3}\mu_e + \frac{1}{2}\mu_3 + \frac{1}{3}\mu_8, \\
\mu_{gu} &= \mu - \frac{2}{3}\mu_e - \frac{1}{2}\mu_3 + \frac{1}{3}\mu_8, \\
\mu_{rs} &= \mu + \frac{1}{3}\mu_e + \frac{1}{2}\mu_3 + \frac{1}{3}\mu_8, \\
\mu_{bu} &= \mu - \frac{2}{3}\mu_e - \frac{2}{3}\mu_8, \\
\mu_{gs} &= \mu + \frac{1}{3}\mu_e - \frac{1}{2}\mu_3 + \frac{1}{3}\mu_8, \\
\mu_{bd} &= \mu + \frac{1}{3}\mu_e - \frac{2}{3}\mu_8.
\end{aligned} \tag{4}$$

We treat the diquark coupling constant G_d as a simple parameter, although the perturbative one-gluon exchange vertex $\mathcal{L}_{\text{int}} = -(g^2/2)\bar{q}\gamma_\mu(\lambda_a/2)q\bar{q}\gamma^\mu(\lambda_a/2)q$, which is valid at extremely high density, tells us that $G_d/G_s = 1/2$ with $N_c = 3$ [33–35]. As a measure of coupling constant G_d , we shall mainly use the gap energy (Δ_0) in the pure CFL phase at $\mu = 500$ MeV and $T = 0$ in the chiral SU(3) limit, as in [11, 23, 24].

We evaluate the thermodynamic potential in the mean-field approximation;

$$\begin{aligned}
\Omega &= \Omega_q + \Omega_e, \\
\Omega_q &= \frac{4}{G_d} \sum_{\eta=1}^3 \Delta_\eta^2 + \frac{N_c}{G_s} \sum_{i=1}^3 (M_i - m_i)^2 \\
&\quad - \frac{T}{2} \sum_n \int \frac{d\mathbf{p}}{(2\pi)^3} \text{tr} \text{Log} [S^{-1}(i\omega_n, \mathbf{p})],
\end{aligned} \tag{5}$$

where

$$\Delta_\eta = \frac{G_d}{8} \langle {}^t q P_\eta q \rangle, \tag{6}$$

$$\begin{aligned}
\mathbf{M} &= \begin{pmatrix} M_u & 0 & 0 \\ 0 & M_d & 0 \\ 0 & 0 & M_s \end{pmatrix} \\
&= \mathbf{m}_0 - \frac{G_s}{2N_c} \begin{pmatrix} \langle \bar{u}u \rangle & 0 & 0 \\ 0 & \langle \bar{d}d \rangle & 0 \\ 0 & 0 & \langle \bar{s}s \rangle \end{pmatrix}, \tag{7}
\end{aligned}$$

are the gap parameter and constituent quark mass matrices. S denotes the 72×72 Nambu-Gor'kov propagator

defined by

$$S^{-1}(i\omega_n, \mathbf{p}) = \begin{pmatrix} \not{p} + \boldsymbol{\mu} \gamma_0 - \mathbf{M} & \sum_\eta P_\eta \Delta_\eta \\ \sum_\eta \bar{P}_\eta \Delta_\eta & {}^t \not{p} - \boldsymbol{\mu} \gamma_0 + \mathbf{M} \end{pmatrix}, \tag{8}$$

with $\not{p} = i\omega_n \gamma_0 - \mathbf{p} \cdot \boldsymbol{\gamma}$. Finally, Ω_e is the contribution from massless electrons

$$\Omega_e = -\frac{\mu_e^4}{12\pi^2} - \frac{\mu_e^2 T^2}{6} - \frac{7\pi^2 T^4}{180}. \tag{9}$$

The optimal values of the variational parameters Δ_η , M and M_s must satisfy the stationary condition (the gap equations);

$$\frac{\partial \Omega}{\partial \Delta_\eta} = 0, \quad \frac{\partial \Omega}{\partial M_{u,d}} = 0 \text{ and } \frac{\partial \Omega}{\partial M_s} = 0. \tag{10}$$

Our task is to search the minimum of the effective potential by solving these gap equations under the local electric and color charge neutrality conditions;

$$\frac{\partial \Omega}{\partial \mu_e} = 0, \quad \frac{\partial \Omega}{\partial \mu_3} = 0 \text{ and } \frac{\partial \Omega}{\partial \mu_8} = 0. \tag{11}$$

For a later convenience, we define here the electron density by

$$n_e = -\frac{\partial \Omega_e}{\partial \mu_e} = \frac{\mu_e^3}{3\pi^2} + \frac{\mu_e T^2}{3}. \tag{12}$$

The formulation made above is a straightforward extension of our previous work [24] to the ($T \neq 0$) case [29, 30].

B. Representation of gap equation and kinetic constraints in terms of quasi-quark wave functions

In this section, we present some analytical way to deal with the gap equation and neutrality constraints. We shall show that the gap equation and neutrality constraints derived above can be further simplified with the aid of the quasi-quark wave functions (spinors). By doing this, not only the physical meanings of these equations become transparent, but also the numerical derivatives can be circumvented. In particular, the latter has a practical advantage because the computations of matrix elements are more favorable than the numerical derivatives.

First, we introduce the Nambu-Gor'kov mean field Hamiltonian density $\mathcal{H}(\mathbf{p}; \boldsymbol{\mu}, \mathbf{\Delta}, \mathbf{M})$ following [11, 23],

$$\Gamma_0 S^{-1}(i\omega_n, \mathbf{p}) \bar{\Gamma}_0 = i\omega_n \mathbf{1}_{72} - \mathcal{H}(\mathbf{p}; \boldsymbol{\mu}, \mathbf{\Delta}, \mathbf{M}). \tag{13}$$

Here we have defined

$$\Gamma_0 = \begin{pmatrix} \gamma_0 \otimes \mathbf{1}_9 & \mathbf{0} \\ \mathbf{0} & \mathbf{1}_{36} \end{pmatrix}, \quad \bar{\Gamma}_0 = \begin{pmatrix} \mathbf{1}_{36} & \mathbf{0} \\ \mathbf{0} & \gamma_0 \otimes \mathbf{1}_9 \end{pmatrix}. \tag{14}$$

$\mathbf{1}_{72}$ denotes the 72-dimensional unit matrix and \mathcal{H} is Hamiltonian density which is also 72×72 matrix in the color, flavor and spinor space. In the same manner as shown in [29], we can lift the spin degeneracy

away from \mathcal{H} as $\mathcal{H} = \mathcal{H}_{36}(p) \otimes P_+ \oplus \mathcal{H}_{36}(-p) \otimes P_-$ with $P_{\pm} \equiv \frac{1 \pm \hat{p} \cdot \boldsymbol{\sigma}}{2}$ being the helicity projectors. $\mathcal{H}_{36}(p)$ has a block-diagonalized form like $\mathcal{H}_{36}(p) = \mathcal{H}_{12}^{(ur,dg,sb)} \oplus \mathcal{H}_8^{(bd,sg)} \oplus \mathcal{H}_8^{(sr,ub)} \oplus \mathcal{H}_8^{(ug,dr)}$. Furthermore, the Nambu-Gor'kov degeneracy is manifest in the latter three blocks; $\mathcal{H}_8^{(\alpha,\beta)} = \mathcal{H}_4^{(\alpha,\beta)} \oplus [-\mathcal{H}_4^{(\alpha,\beta)}]$. Thus we need to know only two matrix structures of $\mathcal{H}_4^{(\alpha,\beta)} \equiv \mathcal{H}_4^{\alpha\beta}$ and $\mathcal{H}_{12}^{(ur,dg,sb)} \equiv \mathcal{H}_{12}^{uds}$ for the evaluation of the effective potential. We

give the explicit form of these matrices below,

$$\mathcal{H}_4^{\alpha\beta} = \begin{pmatrix} M_\alpha - \mu_\alpha & p & 0 & -i\Delta^{\alpha\beta} \\ p & -M_\alpha - \mu_\alpha & -i\Delta^{\alpha\beta} & 0 \\ 0 & i\Delta^{\alpha\beta} & M_\beta + \mu_\beta & -p \\ i\Delta^{\alpha\beta} & 0 & -p & -M_\beta + \mu_\beta \end{pmatrix}, \quad (15)$$

where $\Delta^{\alpha\beta} = \Delta_1, \Delta_2$ and Δ_3 for $(\alpha, \beta) = (bd, sg), (sr, ub)$ and (ug, dr) , respectively, and

$$\mathcal{H}_{12}^{uds} = \begin{pmatrix} M_u - \mu_{ur} & p & 0 & 0 & 0 & 0 & 0 & -i\Delta_3 & 0 & 0 & 0 & -i\Delta_2 \\ p & -M_u - \mu_{ur} & 0 & 0 & 0 & 0 & -i\Delta_3 & 0 & 0 & 0 & -i\Delta_2 & 0 \\ 0 & 0 & M_u + \mu_{ur} & -p & 0 & i\Delta_3 & 0 & 0 & 0 & i\Delta_2 & 0 & 0 \\ 0 & 0 & -p & -M_u + \mu_{ur} & i\Delta_3 & 0 & 0 & 0 & i\Delta_2 & 0 & 0 & 0 \\ 0 & 0 & 0 & -i\Delta_3 & M_d - \mu_{dg} & p & 0 & 0 & 0 & 0 & 0 & -i\Delta_1 \\ 0 & 0 & -i\Delta_3 & 0 & p & -M_d - \mu_{dg} & 0 & 0 & 0 & 0 & -i\Delta_1 & 0 \\ 0 & i\Delta_3 & 0 & 0 & 0 & 0 & M_d + \mu_{dg} & -p & 0 & i\Delta_1 & 0 & 0 \\ i\Delta_3 & 0 & 0 & 0 & 0 & 0 & -p & -M_d + \mu_{dg} & i\Delta_1 & 0 & 0 & 0 \\ 0 & 0 & 0 & -i\Delta_2 & 0 & 0 & 0 & -i\Delta_1 & M_s - \mu_{sb} & p & 0 & 0 \\ 0 & 0 & -i\Delta_2 & 0 & 0 & 0 & -i\Delta_1 & 0 & p & -M_s - \mu_{sb} & 0 & 0 \\ 0 & i\Delta_2 & 0 & 0 & 0 & i\Delta_1 & 0 & 0 & 0 & 0 & M_s + \mu_{sb} & -p \\ i\Delta_2 & 0 & 0 & 0 & i\Delta_1 & 0 & 0 & 0 & 0 & -p & -M_s + \mu_{sb} & 0 \end{pmatrix}. \quad (16)$$

Because the Nambu-Gor'kov degeneracy is not removed, the eigenvalues of this matrix have six sets of the doublet $(\epsilon, -\epsilon)$ corresponding to the energies for a quasi-quark and its Nambu-Gor'kov partner (anti-quasi-quark).

Let us write 18 ($= 72 \div 2 \div 2$) independent eigenvalues of \mathcal{H} as $\{\epsilon_\alpha\}$ with the index α redefined to the label for the quasi-quarks ($\alpha = 1, 2, \dots, 18$) from that for the direct products of color and flavor ($\alpha = ur, dg, sb, db, sg, sr, ub, ug, dr$). Then the thermodynamic potential can be simplified to

$$\begin{aligned}\Omega_q &= \frac{4}{G_d} \sum \Delta_\eta^2 + \frac{N_c}{G_s} \sum (M_i - m_i)^2 \\ &\quad - 2 \sum_{\alpha=1}^{18} \int \frac{d\mathbf{p}}{(2\pi)^3} \left[\frac{|\epsilon_\alpha|}{2} + T \log \left(1 + e^{-|\epsilon_\alpha|/T} \right) \right] \\ &\quad + 2 \sum_{\alpha=1}^{18} \int \frac{d\mathbf{p}}{(2\pi)^3} \frac{p}{2}.\end{aligned}$$

We have subtracted the vacuum contribution in the system with the nine massless quarks. It is difficult to numerically search the minima with respecting the neutrality constraints from this effective potential alone. Therefore, we search them with the aid of the gap equation which is the Δ -derivative of the effective potential. If possible, numerical derivatives should be avoided because the numerical errors associated with them are not well controllable. To avoid them, we express the gap equations in terms of the eigenvectors (eigen-spinors) of \mathcal{H} . First, we simply differentiate Eq. (5) with respect to Δ_n

and equating the result to zero to obtain,

$$\frac{8}{G_d} \Delta_\eta = -T \sum_n \int \frac{d\mathbf{p}}{(2\pi)^3} \text{tr} \left[\frac{1}{i\omega_n \mathbf{1}_{36} - \mathcal{H}_{36}} \frac{\partial \mathcal{H}_{36}}{\partial \Delta_\eta} \right]. \quad (17)$$

Here \mathcal{H}_{36} is the reduced Nambu-Gor'kov Hamiltonian density defined by removing the spin degeneracy from \mathcal{H} as was introduced above. Also we note that the reduced Hamiltonian density takes the form

$$\begin{aligned}
\mathcal{H}_{36} = & \mathcal{H}_0 + M_u \phi_{M_u} + M_d \phi_{M_d} + M_s \phi_{M_s} \\
& + \Delta_1 \phi_1 + \Delta_2 \phi_2 + \Delta_3 \phi_3 \\
& - 3\mu B - \mu_e Q_e - \mu_3 T_3 - \mu_8 T_8,
\end{aligned} \tag{18}$$

with $\mathcal{H}_0 = \mathcal{H}_{36}|_{\mu=0, \Delta=0, M=0}$ being the Hamiltonian density for the system with nine free massless quarks. $\phi_{M_i}, \phi_{\Delta_\eta}$ and $\mathbf{B}, \mathbf{Q}_e, \mathbf{T}_{3,8}$ are the 36×36 matrices with constant matrix elements. These matrices can be obtained by differentiating the reduced Hamiltonian matrix in terms of $M_{u,d}, M_s, \Delta_{1,2,3}, \mu, \mu_{e,3,8}$ as follows.

$$\begin{aligned}
\phi_{M_{u,d}} &= \frac{\partial \mathcal{H}_{36}}{\partial M_{u,d}}, & \phi_{M_s} &= \frac{\partial \mathcal{H}_{36}}{\partial M_s}, \\
\phi_1 &= \frac{\partial \mathcal{H}_{36}}{\partial \Delta_1}, & \phi_2 &= \frac{\partial \mathcal{H}_{36}}{\partial \Delta_2}, & \phi_3 &= \frac{\partial \mathcal{H}_{36}}{\partial \Delta_3}, \\
B &= -\frac{1}{3} \frac{\partial \mathcal{H}_{36}}{\partial \mu}, & Q_e &= -\frac{\partial \mathcal{H}_{36}}{\partial \mu_e}, \\
T_3 &= -\frac{\partial \mathcal{H}_{36}}{\partial \mu_3}, & T_8 &= -\frac{\partial \mathcal{H}_{36}}{\partial \mu_8}.
\end{aligned} \tag{19}$$

Because \mathcal{H}_{36} is an Hermitian matrix for any momentum, we can define the complete set of spinors $\{|p, \alpha, \pm\rangle\}$ by the eigenvalue equation

$$\mathcal{H}_{36}|p, \alpha, \pm\rangle = \pm \epsilon_\alpha(p)|p, \alpha, \pm\rangle, \quad (20)$$

$\alpha = 1, \dots, 18$ and \pm denote the Nambu-Gor'kov charges. Then we have

$$\langle p, \alpha, \pm | \phi_\eta | p, \alpha, \pm \rangle = \pm \frac{\partial \epsilon_\alpha}{\partial \Delta_\eta}, \quad (\eta = 1, 2, 3). \quad (21)$$

Thus we find that Eq. (17) is reduced to

$$\frac{8}{G_d} \Delta_\eta = \sum_{\alpha=1}^{18} \int \frac{d\mathbf{p}}{(2\pi)^3} \tanh\left(\frac{\epsilon_\alpha}{2T}\right) \langle p, \alpha, + | \phi_\eta | p, \alpha, + \rangle,$$

where the Matsubara summation has been performed. In much the same way, we obtain

$$\begin{aligned} \frac{2N_c}{G_s} (M_i - m_i) \\ = \sum_{\alpha=1}^{18} \int \frac{d\mathbf{p}}{(2\pi)^3} \tanh\left(\frac{\epsilon_\alpha}{2T}\right) \langle p, \alpha, + | \phi_{M_i} | p, \alpha, + \rangle. \end{aligned}$$

We remark that, with the aid of these formulae, one can evaluate the gap equation solely with the evaluation of the 18-dimensional eigen-spinors defined by Eq. (20) and some matrix elements in these bases, without recourse to numerical derivatives as is done in [11, 23, 29, 30].

The charge neutrality constraints can be also expressed in terms of the matrix elements in the basis composed of these eigen-spinors. A straightforward application of the above method to $\rho_{3,8} = -\partial \Omega_q / \partial \mu_{3,8} = 0$, $\rho_e^q = -\partial \Omega_q / \partial \mu_e = -n_e$ and $\rho_B = -\frac{1}{3} \partial \Omega_q / \partial \mu$ leads

$$\begin{aligned} 0 &= \sum_{\alpha=1}^{18} \int \frac{d\mathbf{p}}{(2\pi)^3} (2f_F(\epsilon_\alpha) - 1) \langle p, \alpha, + | \mathbf{Q}_{3,8} | p, \alpha, + \rangle, \\ -n_e &= \sum_{\alpha=1}^{18} \int \frac{d\mathbf{p}}{(2\pi)^3} (2f_F(\epsilon_\alpha) - 1) \langle p, \alpha, + | \mathbf{Q}_e | p, \alpha, + \rangle, \\ \rho_B &= \sum_{\alpha=1}^{18} \int \frac{d\mathbf{p}}{(2\pi)^3} (2f_F(\epsilon_\alpha) - 1) \langle p, \alpha, + | \mathbf{B} | p, \alpha, + \rangle. \end{aligned}$$

Here, the Fermi-Dirac distribution function $f_F(\epsilon) = 1/(e^{\epsilon/T} + 1)$ is introduced.

At zero temperature, $f_F(\epsilon) = \theta(-\epsilon)$ so that the net charge will be accumulated in the *blocking region* where $\epsilon < 0$. For the neutrality constraints to be satisfied, there must be the opposite charge density coming from a non-quark sector or from the quark sector with the finite background charge density $\int \frac{d\mathbf{p}}{(2\pi)^3} \sum_\alpha \langle p, \alpha, + | \mathbf{Q} | p, \alpha, + \rangle \neq 0$, which are supplied by tuning the charge chemical potentials μ_e , μ_3 and μ_8 .

For a later convenience, we introduce here a charge generator

$$\tilde{Q} = -Q - T_3 - \frac{1}{2} T_8, \quad (22)$$

the operation of which keeps the CFL state invariant (neutral) and thus represents an unbroken $U(1)$ symmetry in the CFL phase [3]. If we choose the orthogonal

basis of the broken charges (X, Y) in addition to unbroken \tilde{Q} as [10],

$$X = Q + T_3 - 4T_8,$$

$$Y = Q - T_3,$$

the chemical potentials for these charges become

$$\mu_{\tilde{Q}} = -\frac{4}{9}(\mu_e + \mu_3 + \frac{1}{2}\mu_8),$$

$$\mu_X = \frac{1}{18}(-\mu_Q + \mu_3 - 4\mu_8),$$

$$\mu_Y = \frac{1}{2}(-\mu_Q - \mu_3).$$

We find that the matrix representation of \tilde{Q} operator in the 32-dimensional color-flavor mixed Nambu-Gor'kov base is given by

$$\tilde{Q} = -\frac{\partial \mathcal{H}_{36}}{\partial \mu_{\tilde{Q}}} = -\mathbf{Q}_e - \mathbf{T}_3 - \frac{1}{2}\mathbf{T}_8. \quad (23)$$

Because this commutes with the Nambu-Gor'kov Hamiltonian density \mathcal{H}_{36} as it should be, the quasi-particles (eigen-spinors) have definite \tilde{Q} -charges which can be shown to be of integers $(+1, 0, -1)$ [3]. It is also to be noted here, that thermodynamic potential in the quark sector Ω_q does not depend on $\mu_{\tilde{Q}}$ in the fully gapped CFL phase so that it is a \tilde{Q} -insulator [10]. Because of this, the value of $\mu_{\tilde{Q}}$ in the CFL phase ($T = 0$) cannot be determined by the \tilde{Q} neutrality condition in the quark sector; it should be determined completely by the vanishing-point of very gentle slope of potential curvature coming from the electron sector ($\mu_e^3/3\pi^2 = 0$).

III. NUMERICAL RESULTS AND DISCUSSIONS

In this section, we present our numerical results of the solution of the gap equations, and provide the phase diagrams in the (μ, T) -plane for several values of diquark coupling G_d .

Before that, we fix our model parameters. We take the chiral $SU(2)$ limit for the u , d current quark masses ($m_u = m_d = 0$) and $m_s = 80$ MeV [24]. These values might slightly underestimate the effect of the current masses because $m_{u,d}(2\text{ GeV}) = 3\text{-}4$ MeV and $m_s(2\text{ GeV}) = 80\text{-}100$ MeV according to the full lattice QCD simulation [36]. Also we restrict the variational space by putting $M = M_u = M_d$ for simplicity. This simplification does not matter in the chiral symmetry restored phase [29, 30].

For comparison with the previous work [29], we write down the dimensionless parameters adopted in this

Phase	GAP AND MASS PARAMETERS				CONDITIONS FOR CHEMICAL POTENTIALS	GAPLESS QUARK AND \tilde{Q} CHARGE			
	$\Delta_1(ds)$	$\Delta_2(us)$	$\Delta_3(ud)$	M	M_s	$(ur-dg-sb)$	$(db-sg)$	$(ub-sr)$	$(ug-dr)$
CFL (9)	Δ_1	Δ_2	Δ_3	M_s	$[\mu_e = 0]$	all quark modes are fully gapped			
gCFL ₈ (8)	Δ_1	Δ_2	Δ_3	M_s	$\delta\mu_{dbsg} + \frac{M_s^2}{4\mu} \gtrsim \Delta_1$	db			
gCFL (7)	Δ_1	Δ_2	Δ_3	M_s	$\delta\mu_{dbsg(ubsr)} + \frac{M_s^2}{4\mu} \gtrsim \Delta_{1(2)}$	db ub			
uSC (6)		Δ_2	Δ_3	M_s	$[\mu_e = 0]$	$dg-sb$ (1)	(db, sg)		
guSC (5)		Δ_2	Δ_3	M_s	$\delta\mu_{ubsr} + \frac{M_s^2}{4\mu} \gtrsim \Delta_2$	$dg-sb$ (1)	(db, sg)	ub	
2SC (4)			Δ_3	M_s	$[\mu_3 = 0]$	sb	(db, sg)	(ub, sr)	
g2SC (2)			Δ_3	M_s	$[\mu_3 = 0], \delta\mu_{dgur} = \delta\mu_{drug} > \Delta_3$	dg, sb	(db, sg)	(ub, sr)	dr
dSC (6)		Δ_1	Δ_3	M_s		$ur-sb$ (1)		(ub, sr)	
gdSC (5)		Δ_1	Δ_3	M_s	$\delta\mu_{dbsg} + \frac{M_s^2}{4\mu} \gtrsim \Delta_1$	$ur-sb$ (1)	db	(ub, sr)	
2SCus (4)			Δ_2	M_s		dg	(db, sg)		(ub, sr)
UQM (0)				M_s	$[\mu_3 = \mu_8 = 0]$	all quarks are ungapped.			
χ SB (0)				M	M_s	$[\mu_3 = \mu_8 = 0]$	all quarks are massive.		

TABLE I: The nonzero gap parameters, some conditions between gaps and chemical potentials, and the gapless quarks in each phase. The figure in the parenthesis in the first column represents the number of gapped quasi-quark mode. We have defined the $(ai-bj)$ relative chemical potential by $\mu_{aibj} \equiv (\mu_{ai} - \mu_{bj})/2$. “ $dg-sb$ (1)” means that one of the linear combinations, the dg quark and the sb hole remains gapless. The equation for chemical potentials in a bracket must necessarily hold for some symmetry or kinetic reason.

study;

$$m_{u,d}/\Lambda = 0, \quad m_s/\Lambda = 0.1,$$

$$G_S \Lambda^2 \equiv \frac{G_s \Lambda^2}{8N_c} = 2.17.$$

The value of G_s is chosen so that the dynamical quark mass at $\mu = 0$ is 400 MeV for the cutoff $\Lambda = 800$ MeV just for comparison with our previous work [24]. Note, however, that this coupling is a little larger than the value extracted in the NJL model analysis of the meson spectroscopy with instanton induced six-quark coupling [37], i.e., $G_S \Lambda^2 = 1.835$ which is adopted in [29]. We shall perform the calculation with following five different values of the diquark coupling ($G_D \equiv G_d/16$):

1. **extremely weak coupling:**

$$\Delta_0 = 25 \text{ MeV} \leftrightarrow G_D \Lambda^2 = 0.91 \quad (G_D/G_S = 0.42)$$

2. **weak coupling:**

$$\Delta_0 = 80 \text{ MeV} \leftrightarrow G_D \Lambda^2 = 1.37 \quad (G_D/G_S = 0.63)$$

3. **intermediate coupling:**

$$\Delta_0 = 125 \text{ MeV} \leftrightarrow G_D \Lambda^2 = 1.69 \quad (G_D/G_S = 0.78)$$

4. **strong coupling:**

$$\Delta_0 = 160 \text{ MeV} \leftrightarrow G_D \Lambda^2 = 1.92 \quad (G_D/G_S = 0.88)$$

5. **extremely strong coupling:**

$$\Delta_0 = 200 \text{ MeV} \leftrightarrow G_D \Lambda^2 = 2.17 \quad (G_D/G_S = 1.00)$$

The values of G_D/G_S for the intermediate and extremely strong coupling cases are similar to those employed in [29], i.e., $G_D/G_S = 3/4$ and $G_D/G_S = 1$. However,

the following notice is in order here. (i) Our strange quark mass $m_s/\Lambda = 0.1$ is about one half of the value $m_s/\Lambda = 0.23$ adopted in [29]. (ii) We did not included the six-quark interaction which effectively increases the scalar coupling G_S . These two differences make our case favorable to the pairing phases rather than the *unpaired quark matter* (UQM) phase or the *chiral-symmetry broken* (χ SB) phase. In fact, we will see that the phase diagrams for our weak coupling and intermediate coupling cases seem more or less to correspond to those for $G_D/G_S = 3/4$ and $G_D/G_S = 1$ in [29], respectively.

We consider the candidates of phase listed in TABLE I as in [24] in the numerical analyses below.

A. Phases for extremely weak coupling

Let us first discuss the extremely weak coupling case ($\Delta_0 = 25$ MeV). The phase structure in this case is displayed in Fig. 1. At a first glance, we notice that the UQM phase without any symmetry breaking dominates the phase diagram pushing the superconducting phases to the high density regime. This is because the energy gain due to the $\langle \bar{s}s \rangle$ condensation in the UQM phase is larger than the paring energy under the stress as is clarified in [24]. There are also several thermal phase transitions. The thermally-robustest pairing phase is the 2SC and the second phase in this case is the uSC as is found in [29, 30]. In the following, we shall discuss the features of these phase transitions in detail. We first make a close examination on the zero temperature case, and then investigate the finite temperature case.

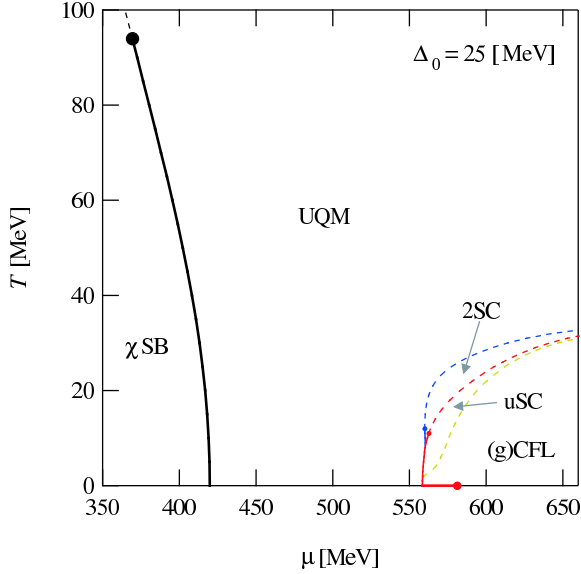


FIG. 1: The phase diagram for the extremely weak coupling ($\Delta_0 = 25$ MeV). Solid (dashed) lines mean first (second) order transitions. Large dot placed on the μ -axis ($\mu = 581.1$ MeV) represents the transition point at which the CFL phase on the high density side continuously turns into the gCFL phase on the low density side.

a. *CFL/gCFL and gCFL/UQM transitions at $T = 0$:* The phases realized at $T = 0$ are the CFL, gCFL and UQM states. In Fig. 2(a), we show the gaps, masses, and chemical potentials along the (g)CFL solution of the gap equation. For $\mu > 558.4$ MeV we confirm that the condensation energy in the (g)CFL solution is largest among those for all the candidates. The excitation gaps of the nine quasi-quarks in the CFL phase are shown in FIG. 2(b). We can see from the figure that one quasi-quark has the largest excitation gap, and other quarks have relatively small gaps. The latter eight modes are the remnants of the color-flavor octet modes in the pure CFL phase at $M_s = 0$. In the CFL phase, the non-vanishing μ_8 and M_s are *dynamically* realized so that the original symmetry of color-flavor diagonal $SU(3)_{C+V}$ is *explicitly* broken down to color $SU(2)_{C+V}$ (color-flavor isospin) in the *Lagrangian level*; because of this, the octet modes split into the isospin-singlet mode (like eta) and two set of doublet (kaonic) modes and the triplet (pionic) modes as $8 \rightarrow 3 (+1, 0, -1) + 2 (+1, 0) + 2 (0, -1) + 1 (0)$ where the associated \tilde{Q} -charge is indicated in the parenthesis. One of the most striking features of the CFL phase is the absence of electrons; the electric neutrality is realized solely by the quark sector $n_u = n_d = n_s$ as can be seen in Fig. 2(c). This CFL phase behaves as \tilde{Q} -insulator because of the absence of gapless \tilde{Q} -carriers [11].

As the density is decreased, the stress energy $-\mu_8(\mu)/2 + M_s^2(\mu)/4\mu$ [11] becomes large in the CFL state. When it reaches $\Delta_1 = \Delta_2$, the first qualitative

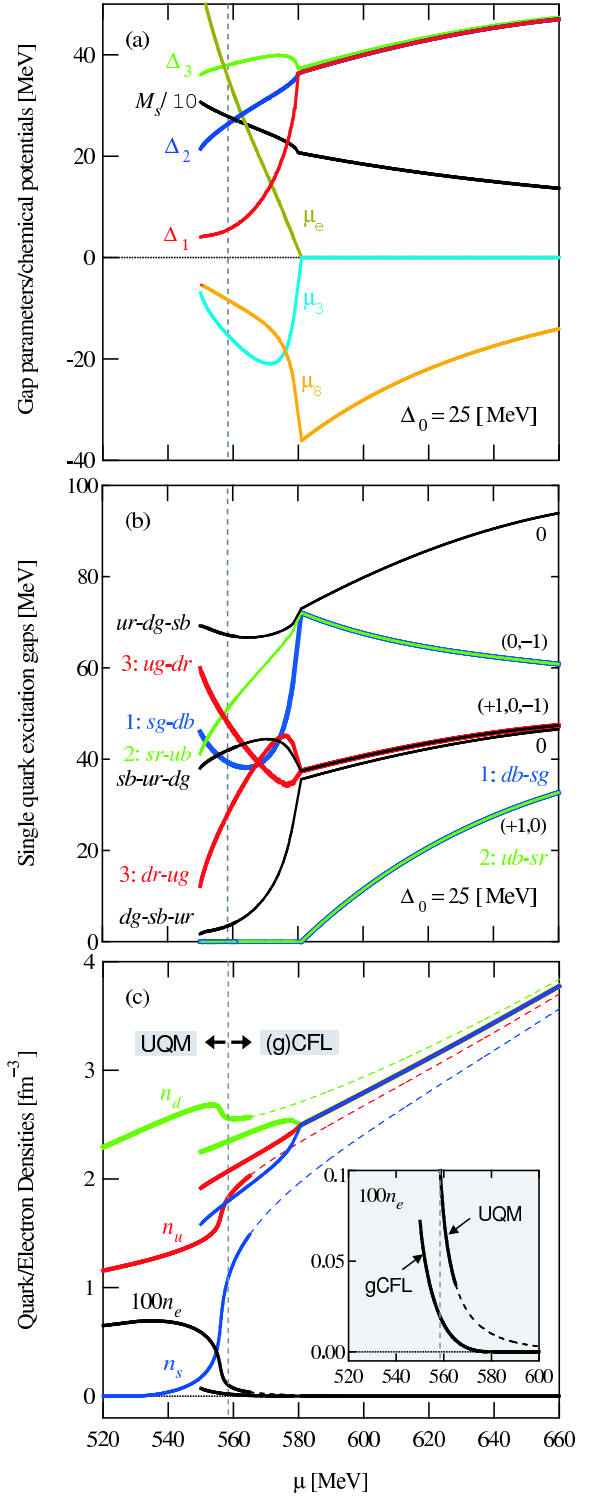


FIG. 2: (a) The (g)CFL solution of the gap equation under the neutrality constraints. The (g)CFL is energetically taken over by the UQM phase on the left side of $\mu = 558.4$ MeV denoted by the vertical dashed line. (b) The excitation gaps in the nine quasi-quark spectra as a function of μ . The \tilde{Q} -charge associated with each mode is also indicated. (c) The quark and electron densities are displayed. The lines on the left hand side are densities in the UQM phase, while those on the right hand side are densities along the (g)CFL solution. The inset shows the density n_e [fm⁻³] on a logarithmic scale versus μ [MeV].

change takes place; this happens when the chemical potential is decreased down to $\mu = 581.1$ MeV. At this point, the CFL state continuously turns into the gCFL phase. Just at the gCFL onset, the excitation gaps for the one doublet modes reaches zero as can be seen in Fig. 2(b). The situation is similar to the K^0 condensation (with a small fraction of K^+ condensation) [38, 39] because the ub - sr and db - sg modes belong to the color-isospin $SU(2)_{C+V}$ doublet, and have $\tilde{Q} = +1$ and 0, respectively.

When the chemical potential is decreased further, the gap parameters split into three different values although they are all still finite. Accordingly, the isospin $SU(2)_{C+V}$ symmetry gets broken by μ_e and μ_3 so that the gaps in quasi-quark dispersions all take different values (see FIG. 2(b)). We remark that the electron chemical potential or its density actually serves as an order parameter of the CFL/gCFL (insulator/metal) transition as claimed in [11].

The gCFL phase continues to be the ground state down to $\mu = 558.4$ MeV below which the UQM phase is more favorable in terms of the thermodynamic potential. When the transition $\text{gCFL} \rightarrow \text{UQM}$ takes place, there should be the large re-configuration of the flavor contents as can be seen in FIG. 2(c). Thus, this transition requires a lot of electro-weak processes which include the d production like $ug(ur) \rightarrow dg(dr) + e^+ + \bar{\nu}_e$ in addition to the decay to the gapless modes accompanied by the electron production $db \rightarrow ub + e^- + \bar{\nu}_e$ and the s quark decay $sb + u \rightarrow db + u$. We should note that there still remains an open interesting question how the UQM droplets are dynamically formed in the gCFL phase and grow against the surface tension.

We have seen that, as the density is decreased, the CFL phase turns into the gCFL phase, and then the gCFL phase gets taken over by the UQM phase. Accordingly, the number of gapped quasi-quark modes decrease as 9 (CFL) \rightarrow 7 (gCFL) \rightarrow 0 (UQM) at $T = 0$ as shown in the previous work [24]. Next, we will discuss how the situation is changed in the $T \neq 0$ case.

b. Phase transitions and crossovers for finite temperature: We show here that the quark matter undergoes a sequence of the transitions, $\text{CFL}(9) \rightarrow \text{gCFL}_8(8) \rightarrow \text{uSC}(6) \rightarrow \text{guSC}(5) \rightarrow \text{2SC}(4) \rightarrow \text{g2SC}(2) \rightarrow \text{UQM}(0)$ as T becomes large; the number of the gapped modes in each phase is indicated with a parenthesis.

In FIG. 3(a), we show the T -dependence of the gaps, masses, and chemical potentials. The figure shows that the Δ_1 first melts and then Δ_2 disappears as T is increased. The thermally-robustest pairing is the 2SC, while second one is the uSC, which is in agreement with the result in [29]. This conclusion will be found to be also consistent with the Ginzburg-Landau analysis given in Sec. III E, where we extend the previous study [22] and see that the large value of the strange quark mass actually disfavors the dSC phase.

In order to study the thermal transition in more detail,

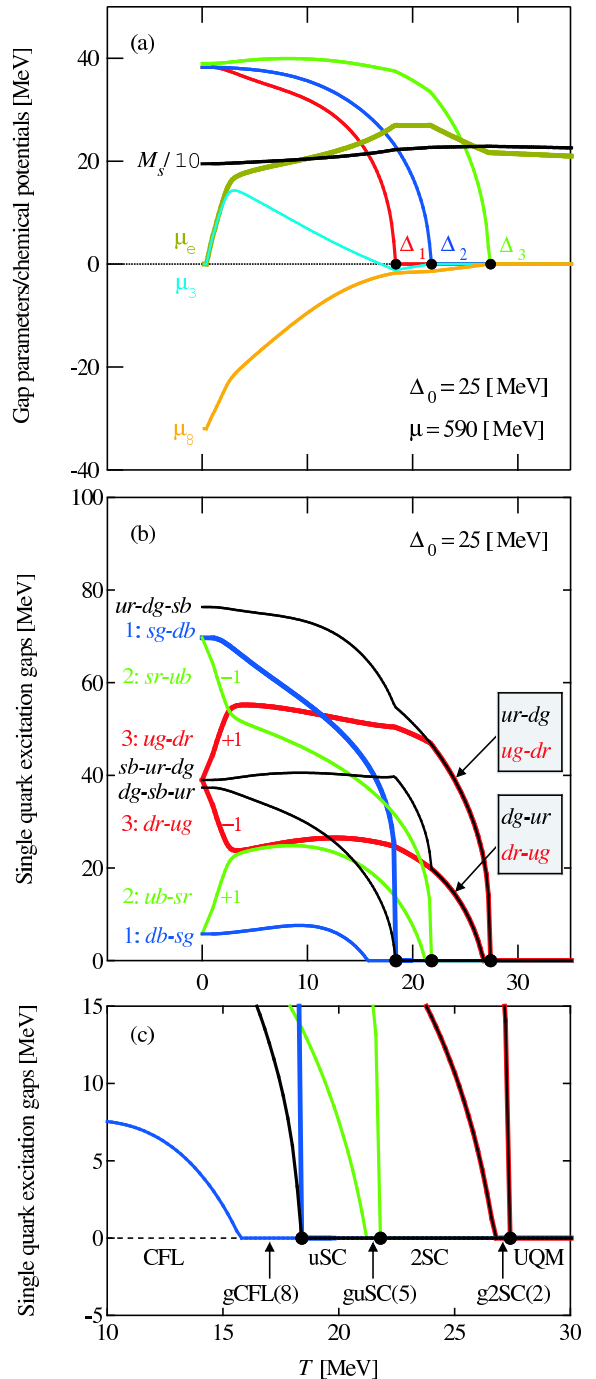


FIG. 3: (a) The gap and mass parameters, and the chemical potentials as a function of T at $\mu = 590$ MeV so that the system at $T = 0$ stays in the CFL phase (see FIG. 2). (b) The nine quasi-quark gaps versus T . Nonzero \tilde{Q} -charge is also indicated by ± 1 . (c) Just an enlargement of the figure (b).

we have also plotted the T -dependence of the gaps in the nine quasi-quark spectra in FIG. 3(b). FIG. 3(c) is just an enlargement of (b). The three large points on the horizontal line indicate $T = T_{cn}$ ($\eta = 1, 2, 3$) at which Δ_η vanishes (the same as the large points in FIG. 3(a)). When the temperature is increased from $T = 0$, the first

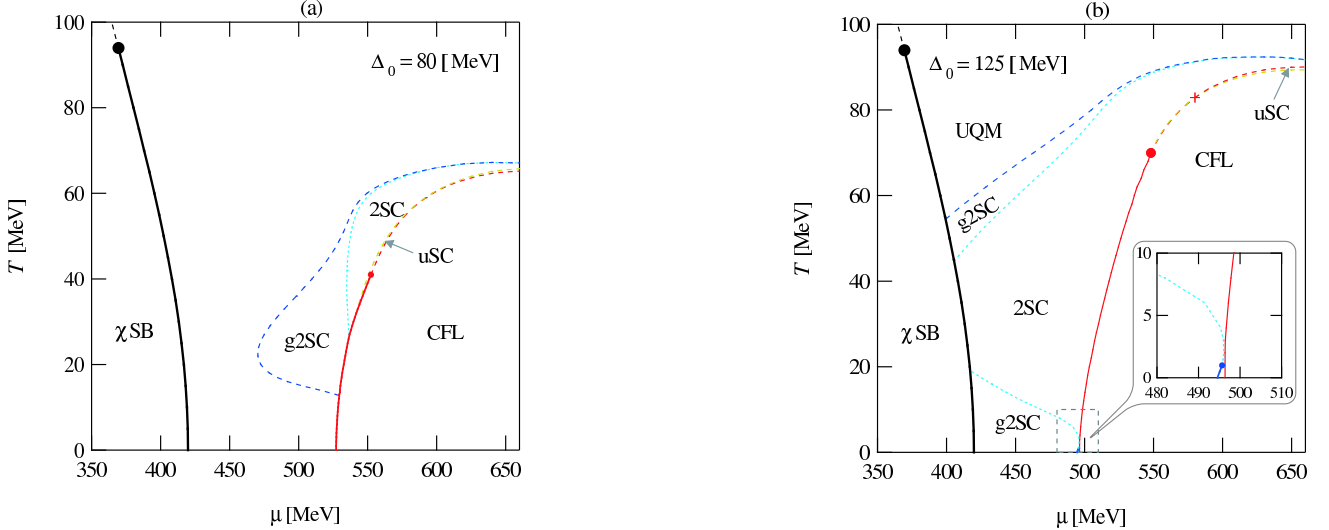


FIG. 4: The phase diagram for the weak coupling ($\Delta_0 = 80$ MeV) (a), and for the intermediate coupling ($\Delta_0 = 125$ MeV) (b).

qualitative change occurs at $T \sim 15.8$ MeV where one of the db - sg dispersion becomes gapless and the gCFL₈ phase (gCFL in [31]) sets in. Unlike the gCFL phase at $T = 0$, the ub - sr dispersion does not become gapless at this point. From the viewpoint of the insulator-to-metal transition, however, the sharp phase transition is smoothen not only due to the absence of the gapless ub - sr mode with $\tilde{Q} = 1$, but also to the thermally-excited on-shell quasi-quarks at finite temperature as the latter ingredient is already noticed in [23]. In fact, from the FIG. 3(b), we can see that the ub - sr ($\tilde{Q} = +1$) mode is lighter than the db - sg ($\tilde{Q} = -1$) mode for $T \lesssim 5$ MeV and accordingly there is a little excess of the quasi-quarks with $\tilde{Q} = +1$ in the system. In order to achieve the neutrality, there must be the equal amount of electrons so that μ_e takes positive finite value as long as T is finite. As a result, the CFL-gCFL₈ (insulator-metal) transition becomes a smooth crossover.

When T is increased further beyond the gCFL₈ onset, Δ_1 disappears at $T \sim 18.4$ MeV. This is a second order phase transition of gCFL₈ \rightarrow uSC. As a consequence, two quasi-quark modes become gapless as is seen in FIG. 3(b); one is the sg - db mode i.e., the partner of the gapless bd - sg mode, while the other is the isospin singlet dg - sb - ur mode.

Next qualitative change occurs when T is increased to $T \sim 21.2$ MeV. At this point, the ub - sr mode with $\tilde{Q} = +1$ becomes gapless and the guSC(5) phase sets in. Notice that because the thermally-excited quasi-quarks are already present in the system over the range ($E_{ub-sr} \lesssim T$), there is no sharp boundary between the uSC(6) and guSC(5) phases.

At a little higher temperature $T \sim 21.8$ MeV, Δ_2 vanishes and above which the 2SC(4) phase is realized. At this transition point, the sr - ub mode having $\tilde{Q} = +1$ becomes gapless. Through the gap parameter Δ_2 , this sr - ub mode is paired with its partner, i.e., the gapless ub - sr

mode. When $\Delta_2 \rightarrow 0$, these two modes get unpaired to become the bare ub and sr quarks. This guSC(5) \rightarrow 2SC(4) phase transition is of second order.

As T is increased further, the crossover 2SC(4) \rightarrow g2SC(2) takes place at $T \sim 26.6$ MeV, and finally the g2SC(2) is taken over by the UQM(0) phase through a second order phase transition at $T \sim 27.4$ MeV.

We have found that the excitation gaps behave in a more complicated manner than the gap parameters as functions of T . However, as we explained, there are no sharp boundary with thermodynamical singularity between CFL(9) and gCFL₈(8), uSC(6) and guSC(5), and 2SC(4) and 2SC(2) transitions. For this reason, we did not indicate these crossover boundaries in the phase diagram of FIG. 1.

B. Phases for weak and intermediate coupling

Let us next examine the weak and intermediate coupling cases ($\Delta_0 = 80$ and $\Delta_0 = 125$ MeV). In FIG. 4, the phase diagrams for the both cases are shown.

1. Phases for the intermediate coupling

We first discuss the case of the intermediate coupling $\Delta_0 = 125$ MeV, in advance of the weak coupling case.

FIG. 4(b) shows that the UQM and gCFL phases disappear at $T = 0$ and the g2SC (CFL) phase exist in the intermediate (high) density regime [24]. We notice that the fully gapped 2SC phase exists in a small μ -region between the CFL and g2SC phases. Also we notice that the transition between the 2SC and g2SC phases is of a first order accompanied by a jump in the dynamical strange quark mass and other physical quantities. This is in contrast to the usual 2SC/g2SC transition without strange

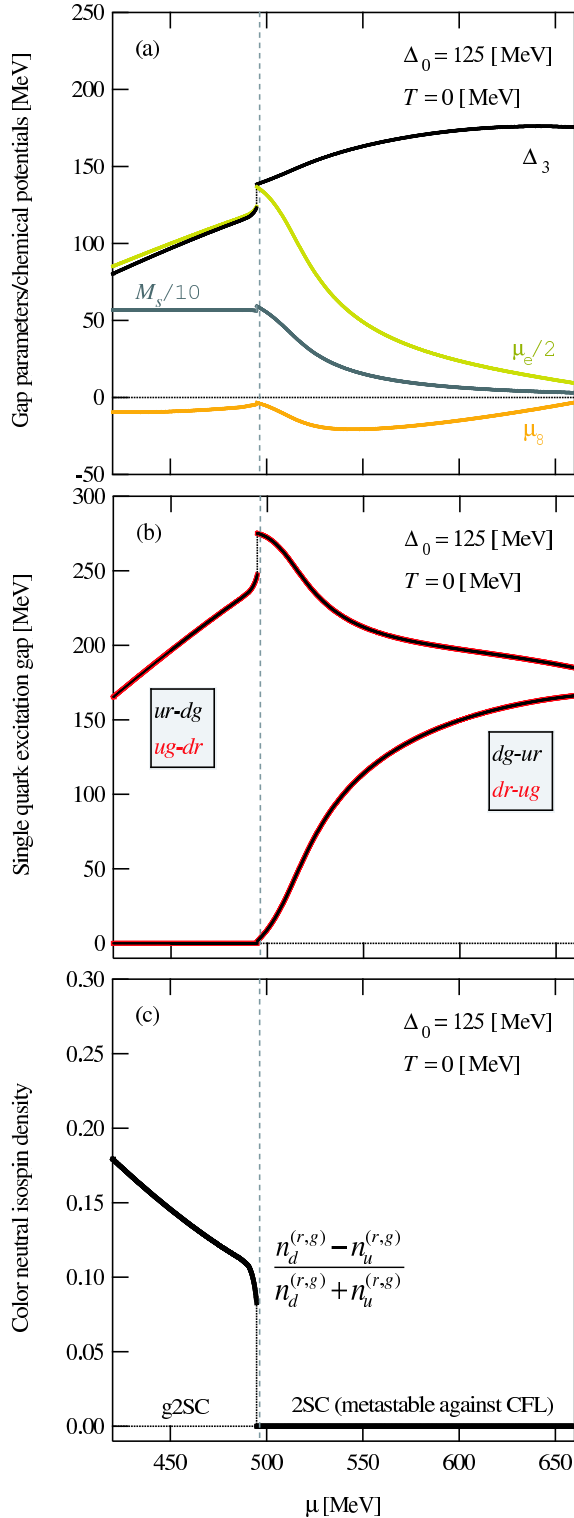


FIG. 5: (a) The gap and mass parameters, and the chemical potentials versus μ along the (g)2SC solution. The dashed line placed on $\mu = 496.4$ MeV represents the point above which the 2SC state is metastable against the CFL. (b) The four quasi-quark gaps as a function of μ . (c) The fraction of the isospin density $\sum_{a=r,g} (n_d^{(r,g)} - n_u^{(r,g)}) / (n_d^{(r,g)} + n_u^{(r,g)})$ to the iso-scalar density $\sum_{a=r,g} (n_u^a + n_d^a)$; by the summation, this quantity is made of neutral with respect to the remaining $SU(2)_{\text{color}}$ charges.

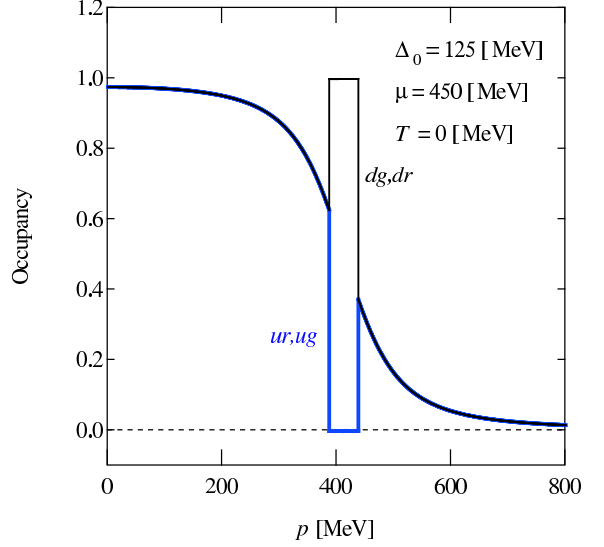


FIG. 6: The occupation number for u and d quarks in the pairing (r, g) sector as a function of momentum p in the g2SC phase at $\Delta_0 = 125$ MeV, $\mu = 450$ MeV and $T = 0$.

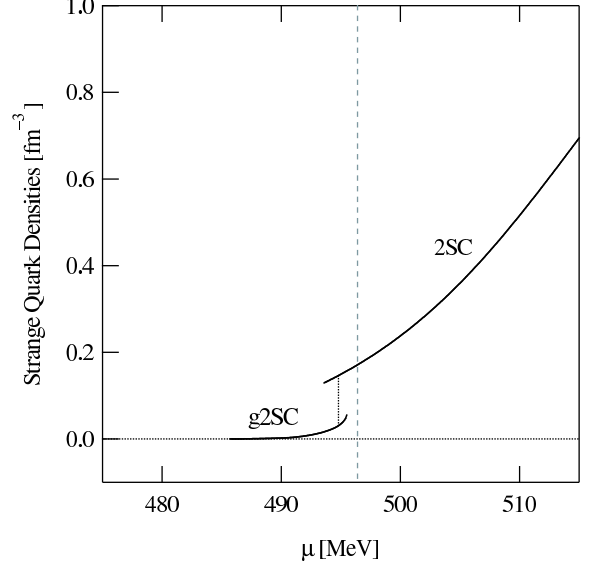


FIG. 7: The strange quark density as a function of μ in the 2SC sector. The vertical dashed line is the same as that in FIG. 5. At $\mu = 498.4$ MeV, the strange quark density jumps accompanying the first order 2SC/g2SC transition.

quarks. We will later discuss this point in detail.

The phases for $T \neq 0$ also differ from the extremely weak coupling case: (i) The window for the uSC phase is pushed away to higher density side and is confined in a small region. The cross placed on the dashed line represents the point at which the window for the uSC phase opens. (ii) The large dot putted on the CFL/2SC transition line indicates the critical endpoint; the dashed line between the large dot and the cross shows that there exists the continuous phase transition of $2\text{SC} \leftrightarrow \text{CFL}$. In

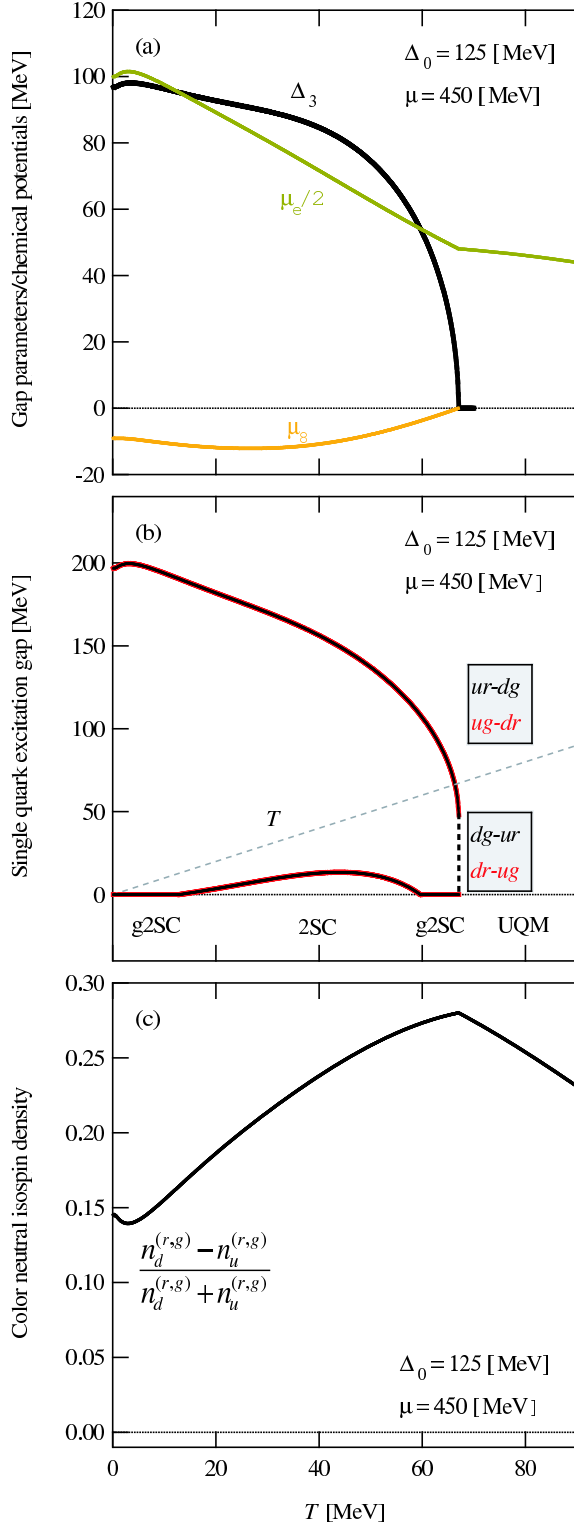


FIG. 8: (a) The gap parameter Δ_3 and the chemical potential $\mu_{e,8}$ versus T for $\Delta_0 = 125$ MeV and $\mu = 450$ MeV. (b) The excitation gaps in the four quasi-quark spectra as a function of T . (c) The $SU(2)_{\text{color}}$ neutral isospin density divided by the total isoscalar density as a function of T . This quantity is an order parameter for the 2SC/g2SC transition at $T = 0$.

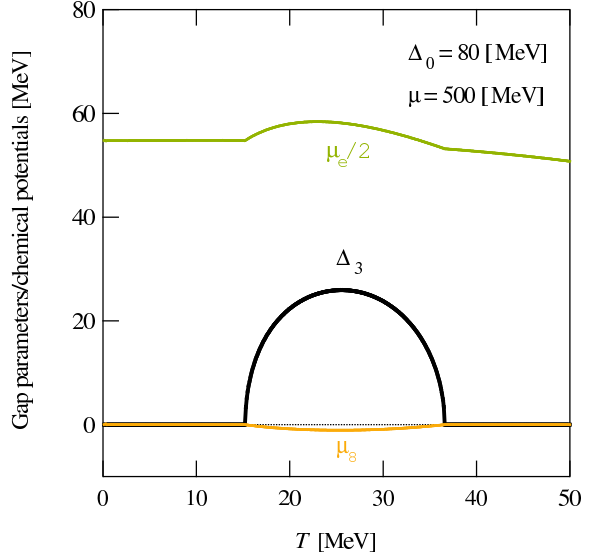


FIG. 9: The gap parameter Δ_3 and the chemical potentials ($\mu_e/2, \mu_8$) versus temperature T at $\mu = 500$ MeV and $\Delta_0 = 80$ MeV; weak coupling case.

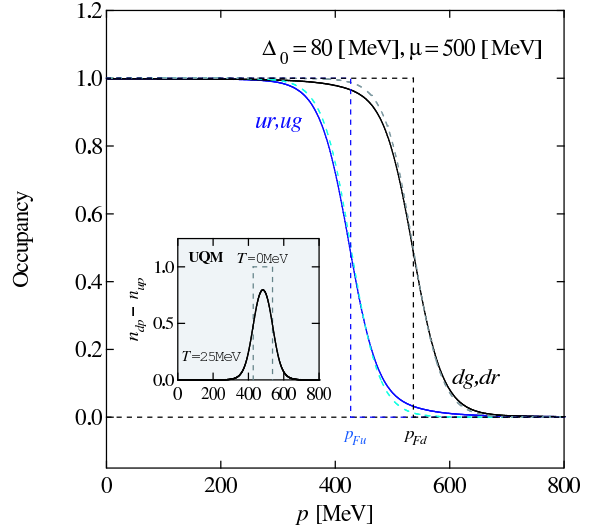


FIG. 10: Solid lines are the occupation numbers for the u and d quarks in the g2SC phase $(\mu, T) = (500 \text{ MeV}, 25 \text{ MeV})$ as a function of momentum p . The sharp Fermi surfaces for the u and d quarks at $T = 0$ are also indicated by the dashed lines. Dashed curves are the u and d occupancies for the unstable UQM phase at $T = 25$ MeV. The inset is the quantity $n_{dp}^{(r,g)} - n_{up}^{(r,g)}$, i.e., the isospin mismatch in the UQM at $T = 0$ (dashed line) and for the unstable UQM at $T = 25$ MeV (solid line).

the following, we shall discuss the detail of the 2SC/g2SC transitions. We first study the $T = 0$ case and then investigate the $T \neq 0$ case.

a. 2SC/g2SC transition at $T = 0$: In FIG. 5(a), we explicitly show the solution of the gap equation in the 2SC sector at $T = 0$. Just to make the argument clear,

we show the 2SC solution for the entire μ -space, but note that the 2SC phase is metastable being energetically taken over by the CFL phase in the right hand side of the vertical dashed line placed on $\mu = 496.4$ MeV; we should keep in mind that the window for the 2SC phase is extremely narrow. Below the critical chemical potential $\mu = 494.8$ MeV, $(\mu_{ug} - \mu_{dr})/2 = (\mu_{ur} - \mu_{dg})/2 = \mu_e/2$ becomes greater than the gap parameter Δ_3 , and as a consequence, the fully gapped 2SC is taken over by the partially ungapped g2SC (See FIG. 5(b)). In FIG. 5(c), the ratio of the $SU(2)_{\text{color}}$ neutral isospin density $\sum_{a=r,g} (n_d^a - n_u^a)$ relative to the isospin scalar density is shown as a function of μ . This quantity serves as an order parameter with which the g2SC phase can be distinguished from the 2SC phase; in the fully gapped 2SC phase, this quantity must be zero because the equal number of u and d quarks are required for the pairing, while in the g2SC phase, the quantity becomes nonzero because of the accumulation of isospin charge in the blocking region. This is clearly seen in the plot of the occupation numbers in the g2SC phase (See FIG. 6). From all the three figures (FIG. 5) in addition to the analyses of the thermodynamic potential, we can conclude that the 2SC/g2SC transition is of first order unlike the usual case without the chiral dynamics, i.e., the $\langle \bar{s}s \rangle$ condensation.

The first order phase transition between these two phases is brought about actually by the competition between the chiral $\langle \bar{s}s \rangle$ condensation and the quark pairing dynamics in the u - d sector as was first recognized in [24]. We can see a small jump in the strange quark mass at the transition point in FIG. 5(a). The strange quark mass reaches almost the vacuum value on the g2SC side, while it varies on the 2SC side and becomes smaller as the density goes high. Accordingly the strange quarks are absent in the g2SC side, while a small number of s quarks are present in the 2SC side and it grows with increasing density. This is naturally understood as follows: In the fully gapped 2SC phase, the $u(rg)$ and $d(rg)$ quark densities should be equal for accommodating the Δ_3 -condensate. Because of the positive electric charge $1/3 = 2/3 - 1/3$ coming from this $SU(2)_{\text{color}}$ sector, the system needs strange quarks, electrons and db -quarks. Thus, the high density condition $[M_s \ll \mu]$ favors the 2SC realization because plenty of strange quarks providing negative charges can exist in the system as can be confirmed by the plot of strange quark density in FIG. 7. But this condition is in turn disfavored with respect to the chiral condensation energy. On the other hand, the g2SC phase can realize the electric neutrality with a less number of strange quarks because of a d quark excess to u quarks in the $SU(2)_{\text{color}}$ sector. Accordingly the g2SC phase is not so much disfavored by the chiral $\langle \bar{s}s \rangle$ condensation ($M_s \gtrsim \mu$) in comparison with the 2SC phase [58]. In short, the g2SC phase can co-exist with the chiral symmetry broken phase easier than the fully gapped 2SC phase can do. The competition of these two ingredients makes the 2SC/g2SC transition be of first order at

$T = 0$.

b. g2SC/2SC/g2SC crossovers for $T \neq 0$: We now investigate how the situation changes for the 2SC/g2SC transition at $T \neq 0$. The phase diagram displayed in FIG. 4(b) shows that, in a relatively low density regime ($430 \text{ MeV} \lesssim \mu \lesssim 480 \text{ MeV}$), the g2SC/2SC and 2SC/g2SC transitions take place successively when the quark matter is heated. This kind of exotic situation is already found in [40] where the systematic study of the coupling strength dependence of the 2SC/g2SC transition is done within the two-flavor NJL model. In our case, the strange quark mass reaches almost its vacuum value in this region so that the pairing dynamics becomes similar to those in the previous two-flavor models. In FIG. 8, we show how the physical quantities behave through these phase transitions for $\mu = 450$ MeV. FIG. 8(a) shows the gap parameters and the chemical potentials as a function of T . $\mu_e/2$ and Δ_3 cross each other twice with increasing T so that the system undergoes the 2SC/g2SC and g2SC/2SC transitions before the pairing is overwhelmed by the UQM. FIG. 8(b) shows the gaps in the quasi-quark spectra. We note, however, that the excitation gap in the dg - ur (dr - ug) quasi-quark spectrum is always smaller than T so that these quasi-quarks are thermally-excited irrespective of whether the system is in the 2SC phase or the g2SC phase. These quasi-quarks smear the 2SC/g2SC and g2SC/2SC transitions. Accordingly, no thermodynamic singularity is associated with these transitions except for the final g2SC-UQM ($\Delta_3 \rightarrow 0$) transition. This can be understood also in terms of the order parameter for the 2SC/g2SC transition at $T = 0$. FIG. 8(c) shows the $SU(2)_{\text{color}}$ neutral isospin density $\sum_{a=r,g} (n_d^a - n_u^a)$ normalized by isoscalar density as a function of T . From the figure, we can see that the g2SC/2SC transitions are crossovers; the order parameter always takes nonzero value and the system is always isospin charged due to the thermally-excited quasi-quarks even for $\mu_e/2 < \Delta_3$ region.

2. Phases for the weak coupling

Now we turn to the weak coupling case ($\Delta_0 = 80$ MeV). The phase diagram is shown in FIG. 4(a). In this case, the diquark coupling is not stronger enough to exclude the UQM phase from $T = 0$, while the gCFL phase is overwhelmed by the UQM with a large $\langle \bar{s}s \rangle$ and thus is washed out as was first noted in the previous work [24].

One of the most striking features in this case is the appearance of the g2SC phase for $T \neq 0$ even when the UQM phase is realized at $T = 0$. This somewhat strange aspect of the color-neutral g2SC phase was first recognized in [40] and has been further confirmed in [23], although it seems that physics for this phenomenon has not yet been clarified enough. In FIG. 9, we show the gap parameter Δ_3 and the chemical potential $(\mu_e/2, \mu_8)$

as a function of T in this situation ($\mu = 500$ MeV). At $T = 0$, the system is in the UQM phase, and the Δ_3 -condensate appears at $T \sim 16$ MeV and then the 2SC turns again into the UQM phase at $T \sim 36.5$ MeV. $\mu_e/2$ is always larger than Δ_3 so that the system is in the “g2SC” phase accompanied by only two gapped quasi-quarks, i.e., the $ur-dg$ and $ug-dr$ modes. However, it should be again noted here that the two phases (2SC and g2SC) are not thermodynamically distinguishable for $T \neq 0$ as explained in the previous section. To understand the appearance of the 2SC phase for $T \neq 0$, we show the occupation number of the u and d quarks for various situations in FIG. 10. There are sharp Fermi surfaces at $T = 0$ which are indicated by dashed lines, i.e., one for d quarks at $p_{Fd} = \mu + \mu_e^{(T=0)}/3$ and the other for u quarks at $p_{Fu} = \mu - 2\mu_e^{(T=0)}/3$. The dashed curves show the u and d quark occupancies at $T = 25$ MeV in the UQM phase which is unstable to the formation of u - d pairs. Quarks are thermally-excited so that the distribution is somewhat smeared. We note that because of this thermal effect, the u and d quarks are under a better kinematical matching than the situation at $T = 0$; from the inset of the figure, we can see that the isospin mismatch ($u_d - u_u$) at the averaged Fermi momentum $p = (p_{Fd} + p_{Fu})/2$ is reduced in the $T = 25$ MeV case from the unity, i.e., the value in the $T = 0$ case. As a result, it is easier for the quark matter in the UQM phase to form the diquark condensate in the isospin singlet channel at finite temperature than at $T = 0$. The solid lines show the occupation numbers after this reconfiguration takes place (the g2SC phase). We remark that unlike the occupation numbers in the g2SC phase at $T = 0$ drawn in FIG. 6, there are no singular points in those for the thermally-smeared g2SC phase for $T \neq 0$.

C. Phases for (extremely) strong coupling

We next discuss the strong and extremely strong coupling cases, $\Delta_0 = 160$ MeV and 200 MeV, respectively. The phase diagrams are depicted in FIG. 11. The phase boundaries move in the directions indicated by the bold arrows when the diquark coupling is increased from $\Delta_0 = 160$ MeV to $\Delta_0 = 200$ MeV. One can see that both the phase structures in these cases are qualitatively identical and are much simpler than those for the weak and intermediate couplings. The premature gapless phases disappear from the low temperature regime, and only the two major pairing phases remain in the phase diagram, i.e., the CFL phase and the 2SC phase. In each case, we still have a small window for the uSC realization as a precursory phase of the $\text{CFL} \rightarrow \text{2SC}$ transition in the high μ -region of the phase diagram. However, one should notice that the critical temperature for the 2SC/UQM transition has a maximum in this chemical potential region, which might imply that this shrinkage of the uSC window is due to a cutoff artifact. It should be also noted that when the diquark coupling is large,

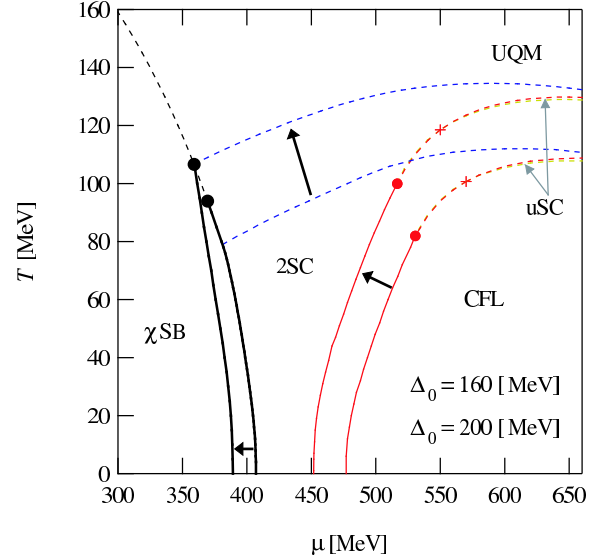


FIG. 11: The phase diagrams for the strong coupling ($\Delta_0 = 160$ MeV) and for the extremely strong coupling ($\Delta_0 = 200$ MeV). Phase boundaries shift in the directions indicated by the bold arrows when the diquark coupling is increased from $\Delta_0 = 160$ MeV to $\Delta_0 = 200$ MeV.

the 2SC phase encroaches upon the domain for the χ SB phase. In addition, the 2SC/UQM transition temperature becomes larger with increasing diquark coupling, and at some critical coupling ($\Delta_0 = \Delta_c$), it reaches the tricritical point of the chiral phase transition: At this coupling, the chiral tricritical point acquires the nature of the doubly critical point where the two second order critical lines merge; one is for the 2SC/UQM transition and the other is for the UQM/ χ SB transition. Because this point has both the tricritical and doubly critical natures, we call it the “TDCP” point. When the diquark coupling is increased beyond this critical coupling Δ_c , the TDCP point shifts to higher temperature because the 2SC/ χ SB transition is always of first order [29]. Our calculation indicates the critical coupling Δ_c where the tricritical point obtains a DCP nature lies between $\Delta_0 = 160$ MeV and $\Delta_0 = 200$ MeV. Finally, it is worth mentioning that in the strong coupling cases discussed above, there is no unstable gapless phase; the phase diagrams in these cases are free from the instability problem associated with imaginary Meissner masses.

D. Baryon density ρ_B at $T = 0$

We have investigated the phase structures of the quark matter in the (μ, T) -plane for several diquark couplings. It is, however, sometimes more convenient to describe the system in the (ρ_B, T) -plane to have a physics intuition into the system. Also it is necessary to have the equation of state as a function of ρ_B to clarify the inner structure of compact stars [30]. Here one should notice

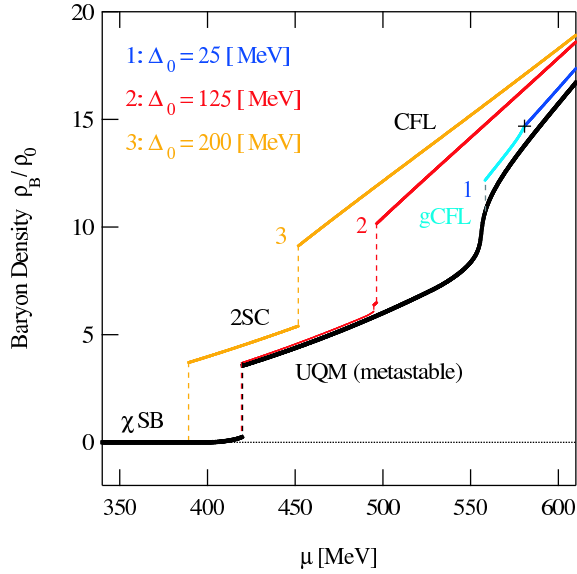


FIG. 12: The baryon number density at $T = 0$ in the unit of $\rho_0 = 0.17 \text{ fm}^{-3}$, i.e., the normal nuclear density. 1, 2, and 3 indicated for each line correspond to the following three cases; the extremely weak coupling ($\Delta_0 = 25 \text{ MeV}$), the intermediate coupling ($\Delta_0 = 125 \text{ MeV}$), and the extremely strong coupling ($\Delta_0 = 200 \text{ MeV}$), respectively. The cross placed on the CFL line indicates the transition point at which the CFL continuously turns into the gCFL phase.

that when multiple phases coexist at a temperature with the same chemical potentials, each phase may have a different baryon density from each other; these phases are actually realized in a mixed phase where the phases with different baryon densities coexist.

Here, we ask how dense each phase at $T = 0$ is. In FIG. 12, we show the baryon density ρ_B versus chemical potential μ at $T = 0$ in the following three cases; (1) the extremely weak coupling $\Delta_0 = 25 \text{ MeV}$, (2) the intermediate coupling $\Delta_0 = 125 \text{ MeV}$ and (3) the extremely strong coupling $\Delta_0 = 200 \text{ MeV}$. In any case, as the chemical potential is lowered from the highest value, the baryon density decreases and shows several jumps associated with first order transitions. We start with the case (1). In this case, the ground state at highest density, about 15 times the normal nuclear matter density, is in the CFL phase. When the density is decreased down to the point indicated by the cross, the CFL continuously turns into the gCFL phase with a steeper gradient $\frac{d\rho}{d\mu} = \frac{1}{\rho} \left(\frac{d\rho}{dP} \right)_T \equiv \kappa_T(\rho)$, i.e., a larger compressibility or equivalently, a larger number fluctuation (susceptibility $\chi_{\rho\rho}^T(r)$) attributed to gapless modes. If the density is decreased further, the first order transition from the gCFL to the UQM takes place; accordingly the baryon density drops down to almost ten times the nuclear density through a mixed phase of the two phases. The UQM phase continues down to ~ 3 times the nuclear density, and then gets taken over by the chiral symmetry broken phase. The situation becomes slightly complicated

in the case (2). The densest phase is again the CFL. As the density is decreased, the CFL phase persists down to almost ten times the nuclear density. Then the quark system undergoes a first order phase transition to the 2SC phase via the dynamical nucleation and growth of the low density 2SC droplets in the CFL phase. This nucleation also needs a lot of weak processes. The density window accommodating the 2SC phase is extremely small and the 2SC phase gets immediately taken over by the g2SC phase. The g2SC phase finally changes into the χ SB phase. Similarly in the case (3), the baryon density drops twice according to the CFL/2SC and 2SC/ χ SB transitions. It is interesting that the lowest baryon density of the CFL phase decreases with increasing diquark coupling while the density at the same μ is enhanced by the factor Δ_0^2/μ^2 . It should be noted, however, that the ρ - μ relation will be affected by the fluctuation effect so that the density becomes even larger due to bosonic degrees of freedom in the strong coupling cases [41].

E. The Ginzburg-Landau analysis

In this section, we make a systematic Ginzburg-Landau analysis in order to understand why the dSC phase does not appear in our calculation of the phase diagram. Our analysis is an extension of the previous work [22]; we expand the Ginzburg-Landau coefficients up to quartic order in M_s which were not taken into account in [22] but turn out to play an important role for the relatively strong coupling (low density) regime. We also notice that this extension makes it possible to provide a unified and systematic description of the thermal pairing/unpairing transitions obtained in the NJL [29] and the Ginzburg-Landau analysis [22].

If the phase transition at finite temperature is of second order where the condensate Δ_η vanishes at the critical point, we can expand the effective potential in terms of the gap parameters near the critical temperature T_c . In this section, we focus on the regime where the chiral symmetry is restored, and assume that the thermal pairing/unpairing transitions are not so much affected by the chiral dynamics there. Thus, we shall switch off the scalar coupling G_s in our NJL lagrangian, Eq. (1), and treat the strange quark mass M_s as a constant parameter. This is nothing but a model used in [23, 42], which will be referred as the *diquark* NJL model hereafter in order to distinguish it from the present NJL model analysis with the scalar coupling, i.e., Eq. (1). Treating M_s as a parameter can be justified by the fact that M_s does not so much vary in the vicinity of T_c (See FIG. 3(a)). Either from the diquark NJL model or from the QCD-like theory with the Cornwall-Jackiw-Tomboulis potential up to 2PI graphs [22], we can derive the Ginzburg-Landau potential. We first emphasize that each of the Ginzburg-Landau coefficients becomes a function of M_s under the neutrality constraints. We evaluate these functions by the Taylor expansion in M_s . Our final task is to cal-

culate the splittings in the critical temperatures up to quartic order in M_s . Here, we shall only give our result for the Ginzburg-Landau potential leaving the detail of the calculation to the Appendix A, because it is some-

what involved although straightforward. After solving the neutrality constraints, the Ginzburg-Landau potential is found to be

$$\begin{aligned} \mathcal{L}_{\text{GL}} = & 4N[\mu]\Delta_1^2 \left(\frac{T - T_{c0}}{T_{c0}} + \frac{M_s^2}{6\mu^2} \log \left(\frac{\mu}{T_{c0}} \right) + \frac{7\zeta(3)M_s^4}{64\pi^2\mu^2T_{c0}^2} \right) \\ & + 4N[\mu]\Delta_2^2 \left(\frac{T - T_{c0}}{T_{c0}} + \frac{7M_s^2}{24\mu^2} \log \left(\frac{\mu}{T_{c0}} \right) + \frac{7\zeta(3)M_s^4}{256\pi^2\mu^2T_{c0}^2} \right) \\ & + 4N[\mu]\Delta_3^2 \left(\frac{T - T_{c0}}{T_{c0}} + \frac{M_s^2}{24\mu^2} \log \left(\frac{\mu}{T_{c0}} \right) + \frac{7\zeta(3)M_s^4}{256\pi^2\mu^2T_{c0}^2} \right) \\ & + \frac{7\zeta(3)N[\mu]}{8\pi^2T_{c0}^2} (\Delta_1^4 + \Delta_2^4 + \Delta_3^4) + \frac{7\zeta(3)N[\mu]}{8\pi^2T_{c0}^2} (\Delta_1^2 + \Delta_2^2 + \Delta_3^2)^2, \end{aligned} \quad (24)$$

where $N[\mu] = \mu^2/2\pi^2$ is the density of state and T_{c0} is the critical temperature for the symmetric ($M_s = 0$) quark matter. Some remarks are in order here. (i) The coefficients for the Δ^4 terms are not expanded in M_s . This is because those effects on the splittings of T_{c0} are small with a suppression factor $(T_{c0}/\mu)^4$ in comparison with the contribution from M_s -dependent terms in the coefficients of Δ^2 terms. (ii) Up to quadratic order in M_s , this exactly coincides with the form obtained in the previous study [22] as it should be [59]. (iii) The M_s^4 -correction to the Ginzburg-Landau coefficient is not so small because it is not a simple expansion in M_s/μ ; the coefficient of M_s^4 is enhanced by factor μ^2/T_{c0}^2 .

We now calculate the splittings of critical temperature $T_{c0} \rightarrow (T_{c1}, T_{c2}, T_{c3})$. We first solve the gap equation

$$\frac{\partial \mathcal{L}_{\text{GL}}}{\partial \Delta_1^2} = 0, \quad \frac{\partial \mathcal{L}_{\text{GL}}}{\partial \Delta_2^2} = 0, \quad \frac{\partial \mathcal{L}_{\text{GL}}}{\partial \Delta_3^2} = 0, \quad (25)$$

in $\Delta_1^2, \Delta_2^2, \Delta_3^2$ and define the temperatures $(T_{\text{ds}}, T_{\text{su}}, T_{\text{ud}})$ as the solutions of $\Delta_1^2(T_{\text{ds}}) = 0, \Delta_2^2(T_{\text{su}}) = 0, \Delta_3^2(T_{\text{ud}}) = 0$. Up to the quartic order in M_s , we obtain

$$\begin{aligned} T_{\text{ds}} &= T_{c0} \left[1 - \log \left(\frac{\mu}{T_{c0}} \right) \frac{M_s^2}{6\mu^2} - \frac{35\zeta(3)\mu^2}{128\pi^2T_{c0}^2} \frac{M_s^4}{\mu^4} \right], \\ T_{\text{su}} &= T_{c0} \left[1 - \log \left(\frac{\mu}{T_{c0}} \right) \frac{2M_s^2}{3\mu^2} + \frac{7\zeta(3)\mu^2}{128\pi^2T_{c0}^2} \frac{M_s^4}{\mu^4} \right], \\ T_{\text{ud}} &= T_{c0} \left[1 + \log \left(\frac{\mu}{T_{c0}} \right) \frac{M_s^2}{3\mu^2} + \frac{7\zeta(3)\mu^2}{128\pi^2T_{c0}^2} \frac{M_s^4}{\mu^4} \right]. \end{aligned} \quad (26)$$

Here we can also see that the M_s^4 -correction could give a significant contribution comparable to the M_s^2 term because of an enhancement factor $\mu^2/T_{c0}^2 \log(\mu/T_{c0})$. We can see that T_{ud} is largest of the three temperatures, which simply means that the 2SC phase is robustest against the thermal disturbance. We can evaluate the critical temperature T_{c3} for the 2SC \rightarrow UQM transition by putting $\Delta_1 = \Delta_2 \rightarrow 0$ in Eq. (24) and solving $\frac{\partial \mathcal{L}}{\partial \Delta_3^2} = 0$

in T . The result is

$$T_{c3} = T_{c0} \left[1 - \log \left(\frac{\mu}{T_{c0}} \right) \frac{M_s^2}{24\mu^2} - \frac{7\zeta(3)\mu^2}{256\pi^2T_{c0}^2} \frac{M_s^4}{\mu^4} \right]. \quad (27)$$

In contrast to the fact that the 2SC is always the hottest pairing phase, the second pairing phase next to the 2SC depends on the value of the strange quark mass. We have to consider the following two cases;

$$\begin{aligned} \text{case [A]} : \quad & M_s^2 < \frac{32\pi^2}{21\zeta(3)} T_{c0}^2 \log(\mu/T_{c0}) \rightarrow T_{\text{su}} < T_{\text{ds}}. \\ \text{case [B]} : \quad & M_s^2 > \frac{32\pi^2}{21\zeta(3)} T_{c0}^2 \log(\mu/T_{c0}) \rightarrow T_{\text{ds}} < T_{\text{su}}. \end{aligned}$$

In case [A], Δ_2 first becomes zero at $T_{\text{su}} \equiv T_{c2}$ and then Δ_1 vanishes at $T_{c1}(> T_{c2})$ when the quark matter is heated from the CFL phase; that is

$$\begin{aligned} T_{c2} &= T_{c0} \left[1 - \log \left(\frac{\mu}{T_{c0}} \right) \frac{2M_s^2}{3\mu^2} + \frac{7\zeta(3)\mu^2}{128\pi^2T_{c0}^2} \frac{M_s^4}{\mu^4} \right], \\ T_{c1} &= T_{c0} \left[1 - \log \left(\frac{\mu}{T_{c0}} \right) \frac{7M_s^2}{24\mu^2} - \frac{49\zeta(3)\mu^2}{256\pi^2T_{c0}^2} \frac{M_s^4}{\mu^4} \right]. \end{aligned} \quad (28)$$

This is actually the case which is studied in [22]; the quark matter undergoes a hierarchical unlocking CFL \rightarrow dSC \rightarrow 2SC \rightarrow UQM. We note, however, that the quartic terms are derived for the first time in this study and these will turn out to be a crucial for a unified picture of the thermal unpairing phase transitions.

Let us now examine the case [B] with a relatively large strange quark mass. In this case, Δ_1 first melts at $T_{c1} = T_{\text{ds}}$ and after that, Δ_2 disappears at $T_{c2}(> T_{c1})$; that is

$$\begin{aligned} T_{c1} &= T_{c0} \left[1 - \log \left(\frac{\mu}{T_{c0}} \right) \frac{M_s^2}{6\mu^2} - \frac{35\zeta(3)\mu^2}{128\pi^2T_{c0}^2} \frac{M_s^4}{\mu^4} \right], \\ T_{c2} &= T_{c0} \left[1 - \log \left(\frac{\mu}{T_{c0}} \right) \frac{13M_s^2}{24\mu^2} - \frac{7\zeta(3)\mu^2}{256\pi^2T_{c0}^2} \frac{M_s^4}{\mu^4} \right]. \end{aligned} \quad (29)$$

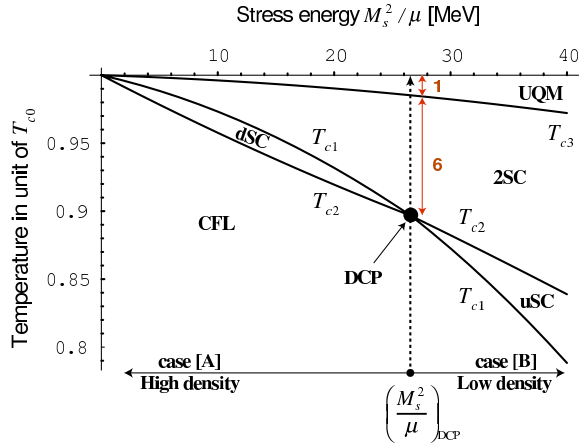


FIG. 13: The plots of $T_{c\eta}$ evaluated by the Ginzburg-Landau analysis with typical parameter set $\Delta_0 = 25$ MeV and $\mu = 500$ MeV. When the coupling strength is increased, the critical DCP stress moves to higher value according to Eq. (34), while the ratio of $T_{c0} - T_{c3} : T_{c0} - T_{DCP} = 1 : 7$ would not be affected within the approximation we are working.

In this case, the quark matter undergoes another hierarchical unlocking $\text{CFL} \rightarrow \text{uSC} \rightarrow \text{2SC} \rightarrow \text{UQM}$.

We have seen that the dSC phase is the second hottest pairing phase in the case [A], while the uSC phase takes over the dSC phase in the case [B]. One can see that the former (latter) situation will be realized at high (low) density. In fact, the case [A] includes the high density situation with the scale hierarchy

$$\frac{M_s^2}{2\mu} \ll M_s \ll (T_{c0}, \Delta_0) \ll \mu, \quad (30)$$

while the case [B] includes the low density regime with the scale hierarchy

$$(T_{c0}, \Delta_0), \frac{M_s^2}{2\mu} \ll M_s \ll \mu. \quad (31)$$

Thus the case [B] contains an interesting regime with $\Delta_0 \sim M_s^2/2\mu$ where the window for the gapless phases open at $T = 0$. These two physically distinct regimes are separated by the *doubly critical point* (DCP) which was first discussed in the numerical analysis of the diquark NJL model [23]. We can analytically derive the critical stress for the DCP point in our current framework as follows;

$$\frac{M_s^2}{2\mu} \Big|_{DCP} (\mu, T_{c0}) = \frac{16\pi^2}{21\zeta(3)} T_{c0} \left(\frac{T_{c0}}{\mu} \right) \log \left(\frac{\mu}{T_{c0}} \right). \quad (32)$$

Just at the density corresponding to this DCP point, we have a simultaneous melting of Δ_1 and Δ_2 , and hence a direct transition $\text{CFL} \rightarrow \text{2SC}$ takes place with increasing T [23]. We can express critical stress for the DCP in terms of the CFL gap Δ_0 at $T = 0$ and $M_s = 0$ with the aid of the weak coupling universal relation

$$T_{c0} = 2^{1/3} \frac{e^\gamma}{\pi} \Delta_0 \cong 0.714 \Delta_0. \quad (33)$$

Thus, the DCP point can be parameterized by the coupling strength Δ_0 as

$$\left(\frac{M_s^2}{2\mu} \right)_{DCP} = \Delta_0 \frac{\Delta_0}{\mu} \left[1.07 + 3.19 \log \left(\frac{\mu}{\Delta_0} \right) \right]. \quad (34)$$

Also, the ratio of T_{c0} to the $\text{CFL} \rightarrow \text{2SC}$ transition temperature at the DCP point which we denote by $T_{DCP} = T_{c1} = T_{c2}$ can be evaluated as

$$\begin{aligned} \frac{T_{DCP}}{T_{c0}} &= 1 - \frac{8\pi^2}{9\zeta(3)} \left[\frac{T_{c0}}{\mu} \log \left(\frac{\mu}{T_{c0}} \right) \right]^2 \\ &= 1 - \left(\frac{\Delta_0}{\mu} \right)^2 \left[0.65 + 1.93 \log \left(\frac{\mu}{\Delta_0} \right) \right]^2. \end{aligned} \quad (35)$$

We can show the ratio

$$T_{c0} - T_{c3}^{[2SC \rightarrow UQM]} : T_{c0} - T_{DCP}^{[\text{CFL} \rightarrow \text{2SC}]} = 1 : 7 \quad (36)$$

is universal being independent of the coupling choice Δ_0 .

FIG. 13 shows the phase diagram calculated with the Ginzburg-Landau potential for $\Delta_0 = 25$ MeV and $\mu = 500$ MeV, where the critical temperatures ($T_{c\eta}$) versus the stress energy (M_s^2/μ) is depicted by changing M_s with μ fixed. The DCP is located at $(M_s^2/\mu)_{DCP} = 26.6$ MeV $\ll \mu = 500$ MeV and $T_c^{DCP}/T_{c0} = 0.90$. These values agree well with those obtained in the numerical analysis of the diquark NJL model where $(M_s^2/\mu)_{DCP} \sim 30$ MeV and $T_c^{DCP}/T_{c0} \sim 0.85$ [23]. If we increase the coupling to $\Delta_0 = (40, 100)$ MeV, then the DCP shifts to $(M_s^2/\mu)_{DCP} = (58.5, 248.4)$ MeV, and $T_c^{DCP}/T_{c0} = (0.81, 0.44)$ according to Eqs. (32) and (35). We can see that the agreement with the diquark NJL result [23] becomes worse in the stronger coupling. This is because M_s^{DCP} shifts to higher value as Δ_0 increases so that the Ginzburg-Landau approach becomes worse due to lack of the scale hierarchy $M_s \ll \mu$. In TABLE II, we have summarized the parameter regime where the Ginzburg-Landau approach and the diquark NJL model are valid. It is worth stressing that according to the Ginzburg-Landau evaluation of the DCP given by Eq. (32), $(M_s^2/\mu)_{DCP}$ is located around $\sim \Delta_0(\Delta_0/\mu)$, which is lower with a factor Δ_{c0}/μ than Δ_{c0} , i.e., the value corresponding to the interesting low density regime $M_s^2/\mu \sim \Delta_0$; the dSC phase is realized at higher density than the gCFL/CFL transition density.

In the following, we discuss where in the (μ, T) -plane the DCP is located. We first discuss the possibility that it is in the moderate density regime using the diquark NJL model. Since the full thermodynamic potential should take the form like $\Omega(\mu, M_s) = T_{c0}^4 f(M_s/\mu, T_{c0}/\mu)$ and T_{c0}/μ is a slowly varying function of μ , changing M_s and changing μ are independent of each other in principle. If we fix M_s to some value, we can obtain the phase diagram in the (μ, T) -plane like FIG. 2 of [42] by determining the phase by changing (μ, T) ; this is contrasted to FIG. 13 where M_s is changed to control the density. In this case, we can find the unique DCP in (μ, T) -plane, which we denote by $(\mu_{DCP}, T_{DCP}) \equiv (\mu, T)_{DCP}$. We note that the

	Regularization scheme	Theoretical parameters	Parameter regime of validity	
Ginzburg-Landau theory	mass counter term	T_{c0}, M_s, μ	$T \sim T_{c0}, \mu \gg M_s, T_{c0}$	high density
Diquark NJL model	momentum cutoff	Λ, G_d, M_s, μ	$\Lambda \gtrsim \mu \gtrsim \mu_{\chi SB}$	moderate density

TABLE II: The comparison of the Ginzburg-Landau theory and the diquark NJL model, i.e., the NJL model without the scalar ($q\bar{q}$)-coupling [11, 23, 42]. In the derivation of the Ginzburg-Landau potential, we adopt the regularization via the mass counter term (Thouless criterion), which insures that all the dimensionful mass scales vanish (correlation length diverges) at T_{c0} when $M_s = 0$. This regularization is model-independent in the sense that, after the prescription, the effective potential have neither Λ -dependence nor the explicit G_d -dependence. The Ginzburg-Landau approach is valid for the weak-coupling regime of QCD at high density ($\mu \gg M_s, T_{c0}$), while the diquark NJL model is expected to describe the non-perturbative regime of ($\Lambda \gtrsim \mu \gtrsim \mu_{\chi SB}$), where $\mu_{\chi SB}$ is the chemical potential for the chiral symmetry restoration.

DCP $(\mu, T)_{DCP}$ shifts in (μ, T) -plane if M_s is changed. We have plotted the DCP $(\mu, T)_{DCP}$ for several choice of M_s in FIG. 14(a). Although we have used the same diquark NJL model as [42], we did not adopted the *chemical potential shift* approximation as is made there, but performed the exact treatment of M_s since the condition $M_s \ll \mu$ does not hold well. As can be seen from the figure, as M_s is increased, the DCP shifts to larger μ pushing away the dSC phase to higher density. We did not find the DCP for $M_s \gtrsim 187$ MeV, where we find only the uSC in the phase diagram. This may be a cutoff artifact because μ_{DCP} increases with increasing M_s and approaches $\Lambda = 800$ MeV.

We have seen that the location of the DCP in the (μ, T) -plane has one-to-one correspondence to the value of M_s . Conversely, if the DCP $(\mu, T)_{DCP}$ is found for some *fixed strange quark mass* M_s , then this M_s can be viewed as the doubly critical strange quark mass M_s^{DCP} for *fixed chemical potential* $\mu = \mu_{DCP}$; this follows from the observation that the dSC (uSC) phase will be realized for $M_s < M_s^{DCP}$ ($M_s > M_s^{DCP}$) as can be expected from FIG. 13. In this sense, we have plotted the doubly critical strange quark mass M_s^{DCP} as a function of μ in FIG. 14(b). For M_s -region above (below) $M_s^{DCP}(\mu)$ line, the uSC (dSC) phase would be realized. Just for comparison, we have also shown the weak coupling Ginzburg-Landau evaluation of the doubly critical strange quark mass, which can be obtained via putting (μ, T_{c0}) -relation into Eq. (32) (see solid line indicated by $M_s^{DCP}(\mu, T_{c0})$). We can see the sizable deviation between these two lines, which is simply attributed to $M_s \not\ll \mu$. However, we stress that the qualitative behaviours are the same; if one goes higher density, the doubly critical strange quark mass shifts to larger value so that the dSC phase becomes robust against the strange quark mass. In order to understand why the dSC does not appear in our model with the scalar coupling G_s and $(q\bar{q})$ -condensates, we have also plotted the dynamically determined strange quark mass in the $\chi SB/UQM$ sector (see the solid line indicated by $M_s^{\chi SB/UQM}$). The dynamical mass is evaluated on the μ - T_{c0} line in FIG. 14(a) so that it should be regarded as the lower limit of the dynamical strange quark mass in the superconducting phase. We can see that the line of $M_s^{\chi SB/UQM}$ is well above the line for $M_s^{DCP}(\mu)$ and the two lines never intersect for $\mu \lesssim \Lambda$, which provides one probable reason for the absence of the dSC in the

present NJL model with dynamical chiral condensates.

Let us finally discuss the possibility that the DCP is located in the weak coupling (μ, T) -regime of QCD. In QCD, it should be unique because the strange quark mass M_s is a decreasing function of μ approaching its current value $m_s \sim 100$ MeV in the high density limit, while the doubly critical strange quark mass M_s^{DCP} is an increasing function of μ . If we assume that the crossing (DCP) point $\mu = \mu^*$ at which $M_s^{DCP}(\mu^*) = M_s(\mu^*)$ is located where $M_s^{DCP}(\mu^*) \ll \mu^*$, then we can estimate μ^* by the weak coupling Ginzburg-Landau result, Eq. (32). By using the universal relation, Eq. (33), and the weak coupling perturbative formula for gap, $\Delta_0(\mu) \sim \mu g^{-5} e^{-\frac{3\pi^2}{\sqrt{2}g}}$ [43, 44] as well, we have the formula $M_s^{DCP} \sim \Delta_0(\mu)/\sqrt{g}$; this is actually a slowly increasing function of μ when g is identified with the running coupling constant $\bar{g}(\mu)$ varying with μ . According to the Schwinger-Dyson analysis of the gap [44–46], $\Delta_0(\mu)/\sqrt{\bar{g}(\mu)}$ reaches ~ 100 MeV around $\mu \sim 10^{10}$ MeV; this indicates μ^* would be located at even higher chemical potential since $m_s \sim 100$ MeV is the lower limit of the mass function $M_s(\mu)$. It should be also noted that our starting assumption $M_s^{DCP}(\mu^*) \ll \mu^*$ can be justified because the weak coupling condition $\Delta_0 < \Delta_0(\mu^*)/\sqrt{\bar{g}(\mu^*)} \ll \mu^*$ is satisfied. We can conclude that the dSC phase is realized in the extremely high density regime of $\mu \gtrsim \mu^*$ of QCD.

IV. SUMMARY AND OUTLOOK

In summary, we have investigated the QCD phase diagram with a special attention to the interplay between the chiral and diquark dynamics for a wide region of the diquark coupling strength. Our results for the two limiting cases, the intermediate and strong coupling, qualitatively agree with those obtained in the recent analyses [29, 30]. Our central results can be summarized as follows. (i) As the diquark coupling is increased, the phase diagram gets gradually dominated by the fully gapped phases, while *premature* gapless phases get excluded out as is noted for $T = 0$ in the previous work [24]. In particular, the phase diagram in the strong diquark coupling ($\Delta_0 \gtrsim 160$ MeV) does not include gapless phases and

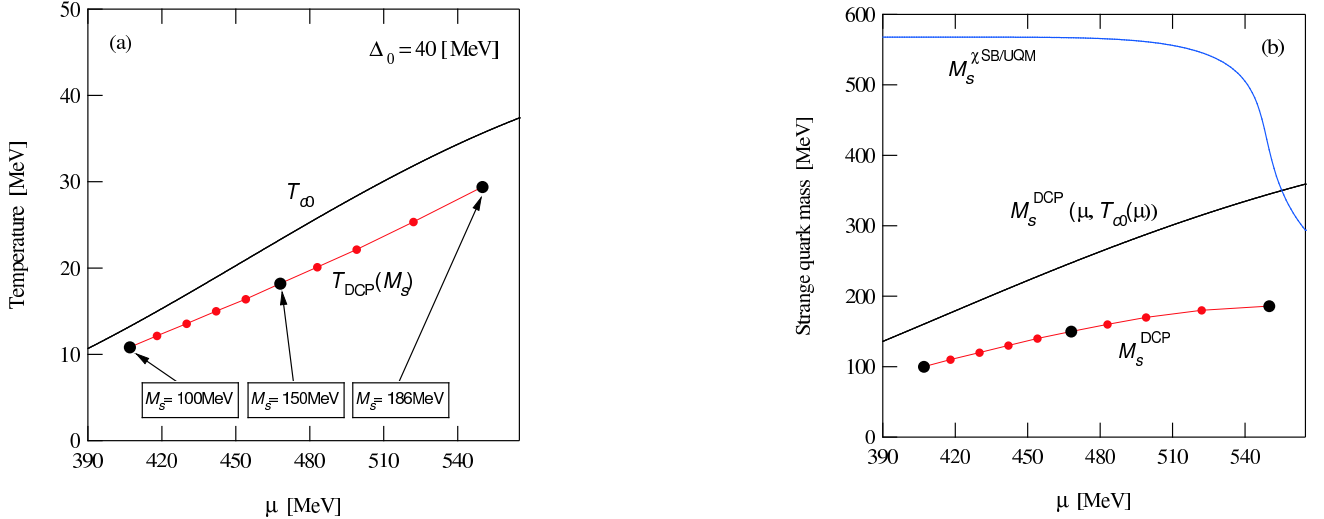


FIG. 14: (a) The DCP point $(\mu, T)_{DCP}$ for various value of M_s ; from left to right, $M_s = 100$ MeV, 110 MeV, \dots , 180 MeV and $M_s = 186$ MeV. The quark-quark coupling G_d is fixed so that $\Delta_0 = 40$ MeV at $\mu = 500$ MeV as in [42]. The solid line is $T_{c0}(\mu)$, i.e., the critical temperature for $M_s = 0$ as a function of μ . (b) The doubly critical strange quark mass M_s^{DCP} as a function of μ . The solid line indicated by $M_s^{DCP}(\mu, T_{c0}(\mu))$ represents the weak coupling Ginzburg-Landau evaluation of M_s^{DCP} by putting the numerical μ - T_{c0} relation depicted in (a) into Eq. (32). The solid line indicated by $M_s^{\chi SB/UQM}$ is the dynamically determined strange quark mass in the χ SB/UQM sector of our model with the scalar ($q\bar{q}$)-coupling.

hence the system is automatically free from the instability problem associated with imaginary Meissner masses. (ii) The second hottest pairing phase next to the 2SC phase depends on the quark density (and also on the diquark coupling strength). In particular, the dSC is not realized for all the parameter regions for which we have performed the calculation. This can be nicely understood by the Ginzburg-Landau analysis incorporating the quartic-order (M_s^4) effects to all the pair susceptibilities. In this analysis, we derived the analytical expression for the doubly critical point (DCP) [23] at which the two second order critical lines intersect; one for the 2SC/dSC transition in the high density side and the other for the 2SC/uSC transition in the low density side. On the basis of this analysis, we conclude that the window for the dSC phase at high density ($T_{c0}, \Delta_0 \gg M_s$) tends to shrink as the density is lowered. (iii) We have demonstrated how and why non-trivial first order transition could be caused by the competition between the diquark and chiral condensations. (iv) We have studied how the 2SC/g2SC and the CFL/gCFL₈ transition is smeared by the thermal disturbance by regarding the electron density and color-neutral isospin density as the order parameters.

In this work, we ignored a Kobayashi-Maskawa-'t Hooft six quark interaction [37, 47, 48], whose effect on the pairing is in part taken into account in [29]. This term, however, also brings a non-trivial interplay between the chiral and diquark dynamics through a mixed contraction like, $|\Delta_3|^2 M_s$, for example; these terms indeed will be induced by the procedure of the mean field approximation. Also we have neglected a possible K^0 condensation in the CFL phase which may be relevant to the instability problem associated with the gapless

phases [49, 50]. Examining this would require a further improvement of our understanding on how the meson spectroscopy on the CFL will be modified by the neutrality constraints [51]. Extending current work so as to take these into account remains indeed an interesting future problem.

A number of papers have been devoted to the resolution of the imaginary Meissner masses in the gapless phases [13, 14]. These include; (i) exploring a possibility of the mixed phase [15] along the line suggested earlier [52–54], (ii) the baryon current generation [16], (iii) examining the crystalline pairing phases [55] taking the neutrality constraints into account [17, 18], (iv) investigating a possible secondary gap formation [19], (v) the gluon condensation in the g2SC [20], and (vi) an inhomogeneous (p -wave) Kaon condensate [21]. Examining all these possibilities or searching for a more stable ground state as well as exploring a nature of the gluonic instability in the gapless phases is now one of central problems in QCD. Apart from this instability problem, we have shown that the chiral dynamics in the strange quark sector may simply wash out all the unstable regime of the gapless phases if the strength of the diquark coupling is large enough. It should be noted, however, that the μ -window for g2SC phase still remains at $T = 0$ in the phase diagram even for the diquark coupling $G_d/G_s = 0.5$, i.e., the value extracted from one gluon exchange vertex. Determining the strength of the in-medium diquark coupling from the phenomenological studies including quark models applied to the exotic baryon spectroscopy as well as the lattice QCD simulation [56] will be needed for a realistic description of the pairing dynamics at low den-

sity.

Acknowledgments

The authors would like to thank M. Kitazawa for discussions at the early stage of this work. H. A. is supported by the Fellowship program, Grant-in-Aid for the 21COE, “Center for Diversity and Universality in Physics” at Kyoto University. T. K. is supported by Grant-in-Aide for Scientific Research by Monbu-Kagakusho (No. 17540250). This work is supported in part by a Grant-in-Aid for the 21st Century COE “Center for Diversity and Universality in Physics”.

APPENDIX A: EVALUATION OF GINZBURG-LANDAU COEFFICIENTS

In this section, we present the detail for a derivation of Eq. (24). We work with the NJL model for a while, but the results will be found to be model-independent by a subtraction of the Thouless criterion: By this subtraction scheme, the model dependence is reduced only to the critical temperature T_{c0} .

We first expand Eq. (5) in terms of Δ at $T \sim T_{c0}$. Up to the quartic order in Δ , we obtain

$$\begin{aligned} \mathcal{L}_{\text{GL}} = & \Omega_e + \frac{4}{G_d} \sum_{\eta=1}^3 \Delta_{\eta}^2 \\ & - T \sum_n \int \frac{d\mathbf{p}}{(2\pi)^3} \text{tr} \log [i\omega_n \mathbf{1} - \mathcal{H}_{36}^0] \\ & + T \sum_{m=1}^4 \frac{1}{m} \sum_n \int \frac{d\mathbf{p}}{(2\pi)^3} \text{tr} \left[\frac{1}{i\omega_n \mathbf{1} - \mathcal{H}_{36}^0} \mathcal{V}_{36} \right]^m, \end{aligned} \quad (\text{A1})$$

where we have defined

$$\mathcal{H}_{36}^0(\mathbf{p}; \mathbf{M}, \boldsymbol{\mu}) = \mathcal{H}_{36}|_{\Delta \rightarrow 0}, \quad \mathcal{V}_{36}(\Delta) = \mathcal{H}_{36} - \mathcal{H}_{36}^0.$$

We omitted the term for the mean-field potential of M_s in Eq. (A1) because we treat it as a constant and as if an external parameter near T_c . The zero-th order term involves the free quark contribution to the thermodynamic potential and the vacuum fluctuation which we shall simply subtract.

$$\begin{aligned} & - T \sum_n \int \frac{d\mathbf{p}}{(2\pi)^3} \text{tr} \log [i\omega_n \mathbf{1} - \mathcal{H}_{36}^0] \\ & = \sum_{a,i} \Omega_0(M_i, \mu_{ai}, T) - 2 \sum_{a,i} \int \frac{d\mathbf{p}}{(2\pi)^3} E_i, \end{aligned} \quad (\text{A2})$$

where $E_i = \sqrt{p^2 + M_i^2}$ and

$$\begin{aligned} \Omega_0(M_i, \mu_{ai}, T) = & -2T \int \frac{d\mathbf{p}}{(2\pi)^3} \log \left(1 + e^{-(E_i - \mu_{ai})/T} \right) \\ & -2T \int \frac{d\mathbf{p}}{(2\pi)^3} \log \left(1 + e^{-(E_i + \mu_{ai})/T} \right). \end{aligned}$$

Because \mathcal{H}_{36} is block-diagonalized as $\mathcal{H}_{36} = \mathcal{H}_{12}^{uds} \oplus \sum_{(\alpha,\beta)}^{(db,sg), (sr,ub), (ug,dr)} [(\mathcal{H}_4^{\alpha\beta}) \oplus (-\mathcal{H}_4^{\alpha\beta})]$, we can evaluate the quadratic and quartic terms for each sector separately as below.

a. $(\mathcal{H}_4^{\alpha\beta}) \oplus (-\mathcal{H}_4^{\alpha\beta})$ sector: For the symmetry reason, we only have the term which is even order in Δ . Thus we have to evaluate the quadratic and quartic terms in Eq. (A1). The quadratic term can be regarded as the static susceptibility. For example, we define $\chi^{(db,sg)}$ for the $(\alpha, \beta) = (db, sg)$ sector by

$$\begin{aligned} & \frac{T}{2} \sum_n \int \frac{d\mathbf{p}}{(2\pi)^3} \text{tr} \left[\frac{1}{i\omega_n \mathbf{1} - \mathcal{H}_4^{\alpha\beta}} \mathcal{V}_4^{\alpha\beta} \right]^2 + (i\omega_n \leftrightarrow -i\omega_n) \\ & = -\Delta_1^2 \chi_{1\text{-loop}}^{(db,sg)}(0, \mathbf{0}; \mu, T, \mu_e, \mu_3, \mu_8, M_s). \end{aligned} \quad (\text{A3})$$

We can analytically evaluate $\chi_{1\text{-loop}}^{(\alpha,\beta)}$ by expanding it in $\vec{t} = (M_s^2/\bar{\mu}_{\alpha\beta}, \delta\mu_{\alpha\beta})$ with $\bar{\mu}_{\alpha\beta} \equiv (\mu_\alpha + \mu_\beta)/2$ and $\delta\mu_{\alpha\beta} \equiv (\mu_\alpha - \mu_\beta)/2$ being referred as the averaged and relative chemical potentials, respectively. Up to quartic order in \vec{t} , we obtain the following expression by performing all the Matsubara summations and the energy integrals except for the term suffering from the UV divergence,

$$\begin{aligned} \chi_{1\text{-loop}}^{(db,sg)} = & 2N[\bar{\mu}_{dbsg}] \left(1 - \frac{M_s^2}{2\bar{\mu}_{dbsg}^2} \right) \int_0 dE \frac{1}{E} \tanh \left(\frac{E}{2T} \right) \\ & - N[\bar{\mu}_{dbsg}] \frac{7\zeta(3)M_s^4}{32\pi^2 \bar{\mu}_{dbsg}^2 T_c^2} \\ & - N[\bar{\mu}_{dbsg}] \frac{7\zeta(3)\delta\mu_{dbsg}M_s^2}{4\pi^2 \bar{\mu}_{dbsg} T_c^2} \\ & - N[\bar{\mu}_{dbsg}] \frac{7\zeta(3)\delta\mu_{dbsg}^2}{2\pi^2 T_c^2}. \end{aligned} \quad (\text{A4})$$

To obtain this, we have ignored the contribution from quasi-antiquark poles. Also we have defined the density of state by $N[\mu] = \mu^2/2\pi^2$.

The term quartic in Δ_1 can also be derived within the same approximation as done in the quadratic term:

$$N[\bar{\mu}_{dbsg}] \left(1 - \frac{3M_s^2}{4\bar{\mu}_{dbsg}^2} \right) \frac{7\zeta(3)\Delta_1^4}{8\pi^2 T_c^2}. \quad (\text{A5})$$

We note that order \vec{t} correction corresponding to the second term in the above expression gives rise to an order M_s^4 correction to the critical temperature $T_{c\eta}$. However it can be shown that this correction to $T_{c\eta}$ is suppressed with a factor $\mathcal{O}(T_{c0}^4/\mu^4)$ in comparison with that from

the t^2 terms in the quadratic term in Eq. (A4). Therefore we shall ignore the second term in Eq. (A5) in the discussion below.

We have demonstrated the expansion in the case of (db, sg) sector, but the Ginzburg-Landau coefficients in other two sectors, (sr, ub) and (ug, dr) , can be derived in the completely same manner.

b. \mathcal{H}_{12}^{uds} sector: Now we take care of the three-flavor mixed sector \mathcal{H}_{12}^{uds} . The terms quadratic in Δ can be shown to have the completely same form as that in the $(\mathcal{H}_4^{\alpha\beta}) \oplus (-\mathcal{H}_4^{\alpha\beta})$ sector. For instance, the term quadratic in Δ_1^2 becomes

$$-\Delta_1^2 \chi_{1\text{-loop}}^{(dg,sb)}, \quad (\text{A6})$$

where $\chi_{1\text{-loop}}^{(dg,sb)}$ is defined by Eq. (A4) with the replacement $(db, sg) \rightarrow (dg, sb)$. On the other hand, the quartic term coming from this sector turns out to be of the exotic form:

$$\begin{aligned} N[\bar{\mu}_{uds}] \frac{7\zeta(3)}{8\pi^2 T_c^2} (\Delta_1^2 + \Delta_2^2 + \Delta_3^2)^2 \\ - N[\bar{\mu}_{uds}] \frac{M_s^2}{\mu_{uds}^2} \frac{21\zeta(3)}{32\pi^2 T_c^2} (\Delta_1^2 + \Delta_2^2)(\Delta_1^2 + \Delta_2^2 + \Delta_3^2), \end{aligned}$$

where we have defined $\bar{\mu}_{uds} \equiv (\mu_{ur} + \mu_{dg} + \mu_{sb})/3$. Also M_s^2 correction can be safely ignored in the analysis below for the same reason as given previously in the non-mixed two flavor sector.

c. Ginzburg-Landau potential: We first investigate the ideal case of $M_s = \mu_{e,3,8} = 0$. Combining all the results above and putting $M_s \rightarrow 0$ and $\mu_{e,3,8} \rightarrow 0$, we have

$$\begin{aligned} \mathcal{L}_{\text{GL}} = \sum_{\eta} \Delta_{\eta}^2 \left[\frac{4}{G_d} - 2\chi_{1\text{-loop}}(0, \mathbf{0}; \mu, T) \right] \\ + (\Delta_1^4 + \Delta_2^4 + \Delta_3^4) N[\mu] \frac{7\zeta(3)}{8\pi^2 T_c^2} \\ + (\Delta_1^2 + \Delta_2^2 + \Delta_3^2)^2 N[\mu] \frac{7\zeta(3)}{8\pi^2 T_c^2}. \quad (\text{A7}) \end{aligned}$$

In this case all the susceptibilities $\chi_{1\text{-loop}}^{(\alpha,\beta)}$ become of the same form and we denoted them by $\chi_{1\text{-loop}}$. The quadratic term is divergent and needs a renormalization. We renormalize it with the use of the gap equation at $T = T_{c0}$ (The Thouless criterion for the critical temperature for three massless quark matter), which plays a role of the mass counter term in [1]:

$$\frac{4}{G_d} = 2\chi_{1\text{-loop}}(0, \mathbf{0}, \mu, T_{c0}). \quad (\text{A8})$$

Subtracting this from the quadratic term, we obtain

$$\begin{aligned} \Delta_{\eta}^2 \left[\frac{4}{G_d} - 2\chi_{1\text{-loop}}(0, \mathbf{0}; \mu, T) \right] \\ \rightarrow 4\Delta_1^2 N[\mu] \int_0 dE \frac{1}{E} \left[\tanh\left(\frac{E}{2T_{c0}}\right) - \tanh\left(\frac{E}{2T}\right) \right] \\ \cong 4\Delta_1^2 N[\mu] \log \frac{T}{T_{c0}} \cong 4\Delta_1^2 N[\mu] \frac{T - T_{c0}}{T_{c0}}. \quad (\text{A9}) \end{aligned}$$

Using this, we obtain

$$\begin{aligned} \mathcal{L}_{\text{GL}} = & (\Delta_1^2 + \Delta_2^2 + \Delta_3^2) 4N[\mu] \frac{T - T_{c0}}{T_{c0}} \\ & + (\Delta_1^4 + \Delta_2^4 + \Delta_3^4) \frac{7\zeta(3)N[\mu]}{8\pi^2 T_{c0}^2} \\ & + (\Delta_1^2 + \Delta_2^2 + \Delta_3^2)^2 \frac{7\zeta(3)N[\mu]}{8\pi^2 T_{c0}^2}. \quad (\text{A10}) \end{aligned}$$

This is exactly of the same form as that obtained earlier in [8, 57].

We now extend this result with the effects of strange quark mass and the charge neutrality constraints taken into account. Our task here is to calculate the splittings of the melting ($\Delta_{\eta} \rightarrow 0$) temperature $T_{c\eta}$ up to the quartic order in M_s . For this purpose, we need the expansion of the Ginzburg-Landau coefficients in terms of variables $t = (M_s^2/\mu, \mu_e, \mu_3, \mu_8)$. In order to derive $T_{c\eta}$ up to the quartic order in M_s , we have to expand the coefficient of the quadratic term up to second order in t . Thus we start with the following Ginzburg-Landau potential.

$$\begin{aligned} \mathcal{L}_{\text{GL}} = & \Omega_e(\mu_e, T_c) + \sum_{ai} \Omega_0(M_i, \mu_{ai}, T_c) \\ & + \Delta_1^2 \left(\frac{4}{G_d} - \chi_{1\text{-loop}}^{(dg,sb)} - \chi_{1\text{-loop}}^{(db,sg)} \right) \\ & + \Delta_2^2 \left(\frac{4}{G_d} - \chi_{1\text{-loop}}^{(sb,ur)} - \chi_{1\text{-loop}}^{(sr,ub)} \right) \\ & + \Delta_3^2 \left(\frac{4}{G_d} - \chi_{1\text{-loop}}^{(ur,dg)} - \chi_{1\text{-loop}}^{(ug,dr)} \right) \\ & + (\Delta_1^4 + \Delta_2^4 + \Delta_3^4) \frac{7\zeta(3)N[\mu]}{8\pi^2 T_{c0}^2} \\ & + (\Delta_1^2 + \Delta_2^2 + \Delta_3^2)^2 \frac{7\zeta(3)N[\mu]}{8\pi^2 T_{c0}^2}. \quad (\text{A11}) \end{aligned}$$

$4/G_d$ in the quadratic terms can again be replaced by $2\chi_{1\text{-loop}}(0, \mathbf{0}, \mu, T_{c0})$ by using the Thouless criterion in the symmetric matter Eq. (A8). By doing this, the model dependence disappears and only its remnant is condensed into the parameter T_{c0} . After this replacement, we can expand the coefficients of Δ_1^2 , Δ_2^2 and Δ_3^2 in $t = (M_s^2/\mu, \mu_e, \mu_3, \mu_8)$. For example, the Δ_1^2 term can be expanded up to second order in t as follows.

$$\begin{aligned}
\Delta_1^2 \left(\frac{4}{G_d} - \chi_{1\text{-loop}}^{(dg, sb)} - \chi_{1\text{-loop}}^{(db, sg)} \right) \rightarrow & N[\mu] \Delta_1^2 \left[\frac{T - T_{c0}}{T_{c0}} \right. \\
& + \left(\frac{2M_s^2}{\mu^2} - \frac{8\mu_e}{3\mu} + \frac{2\mu_3}{\mu} + \frac{4\mu_8}{3\mu} \right) \int_0 dE \frac{1}{E} \tanh \left(\frac{E}{2T_{c0}} \right) \\
& \left. - \left(\frac{3\mu_3 + 2\mu_8 - 4\mu_e}{6\mu} \right)^2 \int_0 dE \frac{1}{E} \tanh \left(\frac{E}{2T_{c0}} \right) + \frac{7\zeta(3)\mu^2}{16\pi^2 T_{c0}^2} \left\{ \frac{M_s^4}{\mu^4} + \left(\frac{\mu_3 - 2\mu_8}{\mu} \right)^2 \right\} \right]. \tag{A12}
\end{aligned}$$

We have used the identity $N[\mu + \delta\mu] = N[\mu] + \mu\delta\mu/\pi^2 + \delta\mu^2/2\pi^2$. Due to the asymmetries between cross-species which is caused by M_s and $\{\mu_e, \mu_3, \mu_8\}$, we cannot completely eliminate the divergent quadratic term by the subtraction of the gap equation at T_{c0} and we still have divergent corrections proportional to

$$\int_0^{\omega_c} dE \frac{1}{E} \tanh \left(\frac{E}{2T_{c0}} \right) = \log \left(\frac{2\omega_c e^\gamma}{\pi T_{c0}} \right), \tag{A13}$$

with γ being the Euler constant and ω_c is a UV cutoff for the quasi-quark energy. We note, however, that this divergence is originated simply in our constant gap parameter ansatz and can be made finite once the momentum dependence of the gap parameter is properly taken into account; it can be shown, in the same manner as

adopted in [22], that we can replace the above divergent contribution by

$$\Delta_\eta^2 \log \left(\frac{2\omega_c e^\gamma}{\pi T_{c0}} \right) \rightarrow \frac{1}{2} \Delta_\eta^2 \log \left(\frac{\mu}{T_{c0}} \right) = \Delta_\eta^2 \frac{3\sqrt{2}\pi^2}{4\bar{g}}, \tag{A14}$$

where Δ_η here should be regarded as the value of the gap energy at the Fermi-momentum $p = \mu$, and \bar{g} is a running gauge coupling constant evaluated at energy scale μ . In the following, we use the above formula instead of ω_c -dependent expression. The Δ_2^2 and Δ_3^2 sectors can be evaluated in the similar way. After combining all the results, we have the full Ginzburg-Landau potential up to the quadratic order in $(M_s^2/\mu, \mu_e, \mu_3, \mu_8)$:

$$\begin{aligned}
\mathcal{L}_{\text{GL}} = & \Omega_e(\mu_e, T_{c0}) + \sum_{ai} \Omega_0(M_i, \mu_{ai}, T_{c0}) \\
& + (\Delta_1^2 + \Delta_2^2 + \Delta_3^2) 4N[\mu] \frac{T - T_{c0}}{T_{c0}} + \frac{7\zeta(3)N[\mu]}{8\pi^2 T_{c0}^2} (\Delta_1^4 + \Delta_2^4 + \Delta_3^4) + \frac{7\zeta(3)N[\mu]}{8\pi^2 T_{c0}^2} (\Delta_1^2 + \Delta_2^2 + \Delta_3^2)^2 \\
& + N[\mu] \left[(\Delta_1^2 + \Delta_2^2) \frac{2M_s^2}{\mu^2} + \frac{4\mu_e}{3\mu} (-2\Delta_1^2 + \Delta_2^2 + \Delta_3^2) + \frac{2\mu_3}{\mu} (\Delta_1^2 - \Delta_2^2) + \frac{4\mu_8}{3\mu} (\Delta_1^2 + \Delta_2^2 - 2\Delta_3^2) \right] \frac{1}{2} \log \left(\frac{\mu}{T_{c0}} \right) \\
& - N[\mu] \left[\Delta_1^2 \left(\frac{3\mu_3 + 2\mu_8 - 4\mu_e}{6\mu} \right)^2 + \Delta_2^2 \left(\frac{3\mu_3 - 2\mu_e - 2\mu_8}{6\mu} \right)^2 + 4\Delta_3^2 \left(\frac{\mu_e - 2\mu_8}{6\mu} \right)^2 \right] \frac{1}{2} \log \left(\frac{\mu}{T_{c0}} \right) \\
& + \frac{7\zeta(3)N[\mu]}{16\pi^2 T_{c0}^2} \mu^2 \left[\Delta_1^2 \left\{ \frac{M_s^4}{\mu^4} + \left(\frac{\mu_3 - 2\mu_8}{\mu} \right)^2 \right\} + \Delta_2^2 \left\{ \left(\frac{\mu_3 + 2\mu_8}{\mu} \right)^2 + \left(\frac{M_s^2}{\mu^2} - \frac{2\mu_e}{\mu} \right)^2 \right\} + 4\Delta_3^2 \left(\frac{\mu_e^2 - \mu_3^2}{\mu^2} \right) \right]. \tag{A15}
\end{aligned}$$

This is one of the central results from which the analytical expression for the splittings of the critical temperature ($T_{c0} \rightarrow T_{c\eta}$) can be derived (see Sec. III E). We now impose the charge neutrality constraints by solving

$$\frac{\partial \mathcal{L}_{\text{GL}}}{\partial \mu_e} = 0, \quad \frac{\partial \mathcal{L}_{\text{GL}}}{\partial \mu_3} = 0, \quad \frac{\partial \mathcal{L}_{\text{GL}}}{\partial \mu_8} = 0, \tag{A16}$$

in μ_e, μ_3, μ_8 . If $\Delta_\eta = 0$, then the first condition above can be casted into the following familiar form of the balance equation under the weak coupling condition ($T \ll \mu$).

$$N_c \left(\frac{2}{3} \frac{p_{Fu}^3}{3\pi^2} - \frac{1}{3} \frac{p_{Fd}^3}{3\pi^2} - \frac{1}{3} \frac{p_{Fs}^3}{3\pi^2} \right) = \frac{\mu_e^3}{3\pi^2}, \tag{A17}$$

with

$$\begin{aligned}
p_{Fu} &= \mu - \frac{2}{3}\mu_e, \\
p_{Fd} &= \mu + \frac{1}{3}\mu_e, \\
p_{Fs} &= \sqrt{(\mu + \frac{1}{3}\mu_e)^2 - M_s^2}. \tag{A18}
\end{aligned}$$

We can solve Eq. (A17) order by order in M_s . Up to the quartic order in M_s , we obtain

$$\mu_e = \frac{M_s^2}{4\mu} - \frac{M_s^4}{48\mu^3}. \tag{A19}$$

We here come back to Eq. (A16), and solve these equations up to the quadratic order not only in M_s^2/μ , but also in Δ_η . We obtain

$$\begin{aligned}\mu_e &= \frac{M_s^2}{4\mu} - \frac{M_s^4}{48\mu^3} - \frac{2\Delta_1^2 - \Delta_2^2 - \Delta_3^2}{6\mu} \log\left(\frac{\mu}{T_{c0}}\right), \\ \mu_3 &= \frac{\Delta_1^2 - \Delta_2^2}{3\mu} \log\left(\frac{\mu}{T_{c0}}\right), \\ \mu_8 &= \frac{\Delta_1^2 + \Delta_2^2 - 2\Delta_3^2}{6\mu} \log\left(\frac{\mu}{T_{c0}}\right).\end{aligned}\quad (\text{A20})$$

Substituting these expression to the free potential $\Omega_e + \sum_{ai} \Omega_0$ and omitting terms which is independent of Δ_η , we have the following Δ_η^4 contribution

$$\frac{8\Delta_1^2(\Delta_2^2 + \Delta_3^2) - 8\Delta_1^4 - 5\Delta_2^4 - 5\Delta_3^4 + 2\Delta_2^2\Delta_3^2}{36\pi^2} \log\left(\frac{\mu}{T_{c0}}\right)^2.$$

Also the feedback contribution to the quartic term comes from the quadratic Δ_η^2 terms in Eq. (A15). Substituting the chemical potentials to the quadratic terms in Eq. (A15) leads to the following quartic terms.

$$\begin{aligned}&\frac{8\Delta_1^4 + 5\Delta_2^2 + 5\Delta_3^4 - 2\Delta_2^2\Delta_3^2 - 8\Delta_1^2(\Delta_2^2 + \Delta_3^2)}{18\pi^2} \log\left(\frac{\mu}{T_{c0}}\right)^2 \\ &- (\Delta_2^2 - \Delta_3^2)(-2\Delta_1^2 + \Delta_2^2 + \Delta_3^2) \frac{7\zeta(3)N[\mu]M_s^2}{48\pi^2\mu^2T_{c0}^2} \log\left(\frac{\mu}{T_{c0}}\right).\end{aligned}$$

These feedback terms bring about the M_s^2 (M_s^4) corrections to the critical temperatures $T_{c\eta}$, but these corrections are $\mathcal{O}(T_{c0}^4/\mu^4)$ suppressed to those from M_s^2 (M_s^4) terms in the susceptibilities. Therefore, we can safely ignore these feedback contribution as long as $\mu \gg T_{c0}$. Substituting Eq. (A20) into the quadratic and quartic terms of Eq. (A15) and picking the parts which survives under $\mu \gg T_{c0}$ lead to our final result for the Ginzburg-Landau potential, i.e., Eq. (24). On the basis of this potential, we can argue how the CFL pairing gets dissolved when T_{c0} is approached as is done in Sec. III E.

In the present framework, we can also give the analytical formula for the following quantity,

$$\left. \frac{\Delta_3^2 - \Delta_2^2}{\Delta_1^2 - \Delta_2^2} \right|_{T \rightarrow T_{c0}} = 2 + \frac{21\zeta(3)}{16\pi^2} \frac{M_s^2}{T_{c0}^2 \log(\mu/T_{c0})} + \dots \quad (\text{A21})$$

We have derived this expression starting with the Ginzburg-Landau potential. Conversely, if the M_s -dependence of this quantity is known, it gives some information about the M_s -dependent terms in the Ginzburg-Landau potential. In [23], this quantity is expanded as $\left. \frac{\Delta_3^2 - \Delta_2^2}{\Delta_1^2 - \Delta_2^2} \right|_{T \rightarrow T_{c0}} = a + b\left(\frac{M_s}{\mu}\right)^2 + c\left(\frac{M_s}{\mu}\right)^4 + \dots$, and the coefficients, a , b and c , are extracted from the numerical result of the diquark NJL model; $a = 2.52$, $b = 36.2$ and $c = 1.02 \times 10^3$ are obtained with a parameter choice $(\mu, \Delta_0) = (500, 25)$ MeV. We find here, however, that Eq. (A21) does not take a form of a simple expansion in $\left(\frac{M_s}{\mu}\right)^2$ but rather seems to be an expansion

in $\frac{M_s^2}{T_{c0}^2 \log(\mu/T_{c0})} = \frac{\mu^2}{T_{c0}^2 \log(\mu/T_{c0})} \left(\frac{M_s}{\mu}\right)^2$. This may explain unusually large numerical values of b and c .

APPENDIX B: OFF-DIAGONAL COLOR DENSITIES

Here, we show that the off-diagonal color densities automatically vanish for the standard ansatz with the diquark condensate, i.e., Eq. (7). To prove this, we include the chemical potentials not only for the diagonal but also for off-diagonal color charges as given in Eq. (3). The Nambu-Gor'kov Hamiltonian density in this case takes the following form after spin-degeneracy removing,

$$\mathcal{H}_{36} = \begin{pmatrix} H_{ur} & D_3 & D_2 & M_{12} & M_{12}^\dagger & M_{45}^\dagger & M_{45}^\dagger \\ D_3 & H_{dg} & D_1 & M_{12} & M_{45} & M_{67} & M_{67}^\dagger \\ D_2 & D_1 & H_{sb} & & & & M_{45}^\dagger \\ M_{12}^\dagger & & & H_{dr} & -D_3 & & \\ M_{12} & & & -D_3 & H_{ug} & M_{67}^\dagger & \\ & M_{45}^\dagger & & & & H_{sr} & -D_2 \\ M_{45} & & M_{67}^\dagger & & M_{67} & -D_2 & M_{12}^\dagger \\ & M_{67}^\dagger & M_{45} & & M_{12} & H_{ub} & \\ M_{67} & & & & & H_{sg} & -D_1 \\ & & & & & -D_1 & H_{db} \end{pmatrix}, \quad (\text{B1})$$

where all the matrix elements are 4×4 matrices defined by

$$\begin{aligned}H_{ia} &= \begin{pmatrix} M_i - \mu_{ai} & p & & \\ p & -M_i - \mu_{ai} & M_i + \mu_{ai} & -p \\ & & -p & -M_i + \mu_{ai} \\ & & -i\Delta_\eta & \end{pmatrix}, \\ D_\eta &= \begin{pmatrix} & & & \\ & i\Delta_\eta & & \\ & & i\Delta_\eta & \\ i\Delta_\eta & & & \end{pmatrix}, \\ M_{\alpha\beta} &= \begin{pmatrix} \mu_\alpha + i\mu_\beta & & & \\ & \mu_\alpha + i\mu_\beta & -\mu_\alpha + i\mu_\beta & \\ & & -\mu_\alpha + i\mu_\beta & -\mu_\alpha + i\mu_\beta \end{pmatrix},\end{aligned}\quad (\text{B2})$$

respectively. We define \mathcal{H}_{36}^0 by putting $\mu_1 = \mu_2 = \mu_4 = \mu_5 = \mu_6 = \mu_7 = 0$ in Eq. (B1).

$$\mathcal{H}_{36}^0 = \begin{pmatrix} H_{ur} & D_3 & D_2 & & & & \\ D_3 & H_{dg} & D_1 & & & & \\ D_2 & D_1 & H_{sb} & & & & \\ & & & H_{dr} & -D_3 & & \\ & & & -D_3 & H_{ug} & & \\ & & & & & H_{sr} & -D_2 \\ & & & & & -D_2 & H_{ub} \\ & & & & & & H_{sg} \\ & & & & & & -D_1 \\ & & & & & & H_{db} \end{pmatrix}, \quad (\text{B3})$$

This Hamiltonian density \mathcal{H}_{36}^0 can be further reduced to the block-diagonalized form as given in the text after some unitary transformation which makes the Nambu-Gor'kov doubling explicit in the (ug, dr) , (db, sg) and (sr, ub) sectors. However this is not necessary in the following argument, so we proceed further with Eq. (B3).

We now define the off-diagonal color charge matrices in the Nambu-Gor'kov bases as

$$\mathbf{Q}_\alpha = -\frac{\partial \mathcal{H}_{36}}{\partial \mu_\alpha}, \quad (\text{B4})$$

with $\alpha = 1, 2, 4, 5, 6, 7$ in addition to the diagonal charges

$$\mathbf{Q}_{e,3,8} = -\frac{\partial \mathcal{H}_{36}}{\partial \mu_{e,3,8}}. \quad (\text{B5})$$

What we have to show is that the off-diagonal color densities automatically vanish on the ground state determined by \mathcal{H}_{36}^0 . To see this, we first define the complete sets by the following eigen-value equation:

$$\mathcal{H}_{36}^0 |p, \alpha, \sigma\rangle^0 = \sigma \varepsilon_\alpha^0(p) |p, \alpha, \sigma\rangle^0. \quad (\text{B6})$$

We have 36 eigenvalues which we distinguish by $\alpha = 1, 2, \dots, 18$ and the Nambu-Gor'kov spin $\sigma = \pm$. The off-diagonal color densities can be written in the form as in Sec. II B,

$$\begin{aligned} \rho_\alpha &= -\frac{1}{2} \sum_{\alpha=1}^{18} \int \frac{d\mathbf{p}}{(2\pi)^3} \tanh\left(\frac{\varepsilon_\alpha^0}{2T}\right)^0 \langle p, \alpha, + | \mathbf{Q}_\alpha | p, \alpha, + \rangle^0 \\ &+ \frac{1}{2} \sum_{\alpha=1}^{18} \int \frac{d\mathbf{p}}{(2\pi)^3} \tanh\left(\frac{\varepsilon_\alpha^0}{2T}\right)^0 \langle p, \alpha, - | \mathbf{Q}_\alpha | p, \alpha, - \rangle^0. \end{aligned} \quad (\text{B7})$$

The $\tilde{\mathbf{Q}}$ charge matrix in the Nambu-Gor'kov bases

$$\tilde{\mathbf{Q}} = -\mathbf{Q}_e - \mathbf{Q}_3 - \frac{1}{2} \mathbf{Q}_8 \quad (\text{B8})$$

commutes with the Hamiltonian density \mathcal{H}_{36}^0 , i.e., $[\mathcal{H}_{36}^0, \tilde{\mathbf{Q}}] = 0$, so that the quasi-particle states $|p, \alpha, \pm\rangle^0$ can be chosen to be the eigenstates of $\tilde{\mathbf{Q}}$. Also we note

$$\begin{aligned} \mathbf{Q}_1 &= -i[\tilde{\mathbf{Q}}, \mathbf{Q}_2], \\ \mathbf{Q}_2 &= +i[\tilde{\mathbf{Q}}, \mathbf{Q}_1], \\ \mathbf{Q}_4 &= -i[\tilde{\mathbf{Q}}, \mathbf{Q}_5], \\ \mathbf{Q}_5 &= +i[\tilde{\mathbf{Q}}, \mathbf{Q}_4]. \end{aligned} \quad (\text{B9})$$

From these commutation relations, we can immediately conclude

$$\rho_1 = \rho_2 = \rho_4 = \rho_5 = 0, \quad (\text{B10})$$

because

$${}^0 \langle p, \alpha, \sigma | \mathbf{Q}_1 | p, \alpha, \sigma \rangle^0 = i {}^0 \langle p, \alpha, \sigma | [\mathbf{Q}_2, \tilde{\mathbf{Q}}] | p, \alpha, \sigma \rangle^0 = 0 \quad (\text{B11})$$

This conclusion follows from $\tilde{\mathbf{Q}}$ is diagonal in the quasi-particle bases,

$${}^0 \langle p, \alpha, \sigma | \tilde{\mathbf{Q}} | p, \beta, \sigma' \rangle^0 = q_\alpha^\sigma \delta_{\alpha\beta} \delta_{\sigma\sigma'}, \quad (\text{B12})$$

where q_α^σ takes the values $(-1, 0, +1)$.

In contrast, the disappearances of ρ_6 and ρ_7 cannot be proven in the same manner because of the commutation relations:

$$i[\tilde{\mathbf{Q}}, \mathbf{Q}_6] = 0, \quad i[\tilde{\mathbf{Q}}, \mathbf{Q}_7] = 0. \quad (\text{B13})$$

Thus we try to give a more direct proof here. We first re-write Eq. (B7) as

$$\begin{aligned} \rho_\alpha &= -\frac{1}{2} \sum_{\sigma, \alpha} \int \frac{d\mathbf{p}}{(2\pi)^3} {}^0 \langle p, \alpha, \sigma | \tanh\left(\frac{\mathcal{H}_{36}^0}{2T}\right) \mathbf{Q}_\alpha | p, \alpha, \sigma \rangle^0 \\ &= -\frac{1}{2} \sum_{\sigma, \alpha} \int \frac{d\mathbf{p}}{(2\pi)^3} \text{tr} \left[\tanh\left(\frac{\mathcal{H}_{36}^0}{2T}\right) \mathbf{Q}_\alpha \right]. \end{aligned} \quad (\text{B14})$$

Since the trace does not depend on the base, we can evaluate the trace with the *natural* base instead of the quasi-particle eigen-spinors. Thus what we have to show here turns out to be the proof of

$$\text{tr} [\mathcal{H}_{36}^0 \mathbf{Q}_{6,7}] = 0, \quad \text{tr} [\mathcal{H}_{36}^0 \mathcal{H}_{36}^0 \mathcal{H}_{36}^0 \mathbf{Q}_{6,7}] = 0, \dots. \quad (\text{B15})$$

If this infinite series of conditions can be shown to be true, then we can conclude

$$\rho_6 = \rho_7 = 0. \quad (\text{B16})$$

Using the explicit form of the matrices \mathcal{H}_{36}^0 and $\tilde{\mathbf{Q}}_{6,7}$, we have explicitly checked using the *Mathematica*, that the equation

$$\text{tr} [(\mathcal{H}_{36}^0)^{2n-1} \mathbf{Q}_{6,7}] = 0 \quad (\text{B17})$$

indeed holds for $n = 1, 2, \dots, 18$. We have not confirmed Eq. (B17) for $n > 18$, but the confirmation up to $n \leq 18$ is adequate for the reason we shall give in the following.

First, we write the Hamiltonian density

$$\mathcal{H}_{36}^0 = \sum_{\sigma, \alpha} \sigma \varepsilon_\alpha(p) P_{\sigma\alpha} = \sum_{\alpha=1}^{18} (P_\alpha - P_{-\alpha}) \varepsilon_\alpha(p), \quad (\text{B18})$$

where $P_{\sigma\alpha}$ is the projection operator $|p, \alpha, \sigma\rangle^0 \langle p, \alpha, \sigma|$ in the natural base; this operator projects vectors out to the eigenspace in which $\mathcal{H}_{36}^0 = \sigma \varepsilon_\alpha(p)$ holds. Using this decomposition, we can re-write the 18 conditions as

$$\begin{aligned} 1 : 0 &= \sum_{\alpha=1}^{18} \varepsilon_\alpha \text{tr} [(P_\alpha - P_{-\alpha}) \mathbf{Q}_{6,7}], \\ 2 : 0 &= \sum_{\alpha=1}^{18} \varepsilon_\alpha^3 \text{tr} [(P_\alpha - P_{-\alpha}) \mathbf{Q}_{6,7}], \\ &\vdots \\ 18 : 0 &= \sum_{\alpha=1}^{18} \varepsilon_\alpha^{35} \text{tr} [(P_\alpha - P_{-\alpha}) \mathbf{Q}_{6,7}]. \end{aligned} \quad (\text{B19})$$

If all the eighteen roots $\{\varepsilon_\alpha\}$ with $\alpha = 1, 2, \dots, 18$ take different values, then the above eighteen conditions simply mean

$$\text{tr} [(P_\alpha - P_{-\alpha}) \mathbf{Q}_{6,7}] = 0, \quad (\text{B20})$$

for $\alpha = 1, 2, \dots, 18$. Therefore for the arbitrary integer n , $\text{tr}[(\mathcal{H}_{32}^0)^{2n-1} \mathbf{Q}_{6,7}] = 0$ should hold. In the case that the degeneracy is present as $\varepsilon_1 = \varepsilon_2 = \varepsilon_3$, for example, we can prove the following equation in the totally same manner as in the above argument,

$$\sum_{\alpha=1,2,3} \text{tr} [(P_\alpha - P_{-\alpha}) \mathbf{Q}_{6,7}] = 0, \quad (\text{B21})$$

and again reach the same conclusion $\text{tr}[(\mathcal{H}_{32}^0)^{2n-1} \mathbf{Q}_{6,7}] =$

0. Thus, we have proven that the following condition indeed holds for $\alpha = 6$ and 7,

$$\text{tr} \left[\tanh \left(\frac{\mathcal{H}_{36}^0}{2T} \right) \mathbf{Q}_\alpha \right] = 0. \quad (\text{B22})$$

Consequently, we reached the fact that all the off-diagonal color densities automatically vanish under the assumption of the diquark condensate given in Eq. (7).

[1] D. Bailin and A. Love, Phys. Rept. **107** (1984) 325.
[2] M. Iwasaki and T. Iwado, Phys. Lett. B **350** (1995) 163.
[3] For reviews, see K. Rajagopal and F. Wilczek, arXiv:hep-ph/0011333; M. G. Alford, Ann. Rev. Nucl. Part. Sci. **51**, 131 (2001) [arXiv:hep-ph/0102047]; G. Nardulli, Riv. Nuovo Cim. **25N3**, 1 (2002) [arXiv:hep-ph/0202037]; S. Reddy, Acta Phys. Polon. B **33**, 4101 (2002) [arXiv:nucl-th/0211045]; T. Schäfer, arXiv:hep-ph/0304281; M. Alford, Prog. Theor. Phys. Suppl. **153**, 1 (2004) [arXiv:nucl-th/0312007].
[4] M. G. Alford, K. Rajagopal and F. Wilczek, Nucl. Phys. B **537**, 443 (1999) [arXiv:hep-ph/9804403].
[5] M. G. Alford, J. Berges and K. Rajagopal, Nucl. Phys. B **558** (1999) 219 [arXiv:hep-ph/9903502].
[6] T. Schäfer and F. Wilczek, Phys. Rev. D **60**, 074014 (1999) [arXiv:hep-ph/9903503].
[7] H. Abuki, Prog. Theor. Phys. **110**, 937 (2003) [arXiv:hep-ph/0306074].
[8] K. Iida and G. Baym, Phys. Rev. D **63**, 074018 (2001) [Erratum-ibid. D **66**, 059903 (2002)] [arXiv:hep-ph/0011229].
[9] K. Rajagopal and F. Wilczek, Phys. Rev. Lett. **86**, 3492 (2001) [arXiv:hep-ph/0012039].
[10] M. Alford and K. Rajagopal, JHEP **0206**, 031 (2002) [arXiv:hep-ph/0204001].
[11] M. Alford, C. Kouvaris and K. Rajagopal, Phys. Rev. Lett. **92**, 222001 (2004) [arXiv:hep-ph/0311286]; Phys. Rev. D **71**, 054009 (2005) [arXiv:hep-ph/0406137].
[12] M. Alford, P. Jotwani, C. Kouvaris, J. Kundu and K. Rajagopal, Phys. Rev. D **71**, 114011 (2005) [arXiv:astro-ph/0411560].
[13] M. Huang and I. A. Shovkovy, Phys. Rev. D **70**, 094030 (2004) [arXiv:hep-ph/0408268]; Phys. Rev. D **70** (2004) 051501 [arXiv:hep-ph/0407049]; R. Casalbuoni, R. Gatto, M. Mannarelli, G. Nardulli and M. Ruggieri, Phys. Lett. B **605** (2005) 362 [Erratum-ibid. B **615** (2005) 297] [arXiv:hep-ph/0410401]; I. Giannakis and H. C. Ren, Phys. Lett. B **611** (2005) 137 [arXiv:hep-ph/0412015]; Nucl. Phys. B **723**, 255 (2005) [arXiv:hep-th/0504053]; for a general argument on the emergence of the imaginary Meissner mass in a gapless phase, see, M. Alford and Q. h. Wang, J. Phys. G **31** (2005) 719 [arXiv:hep-ph/0501078].
[14] K. Fukushima, Phys. Rev. D **72**, 074002 (2005) [arXiv:hep-ph/0506080].
[15] S. Reddy and G. Rupak, Phys. Rev. C **71** (2005) 025201 [arXiv:nucl-th/0405054].
[16] M. Huang, arXiv:hep-ph/0504235.
[17] R. Casalbuoni, R. Gatto, N. Ippolito, G. Nardulli and M. Ruggieri, Phys. Lett. B **627**, 89 (2005) [arXiv:hep-ph/0507247].
[18] I. Giannakis, D. f. Hou and H. C. Ren, Phys. Lett. B **631**, 16 (2005) [arXiv:hep-ph/0507306].
[19] D. K. Hong, arXiv:hep-ph/0506097; M. Alford and Q. h. Wang, arXiv:hep-ph/0507269.
[20] E. V. Gorbar, M. Hashimoto and V. A. Miransky, arXiv:hep-ph/0507303; arXiv:hep-ph/0509334.
[21] T. Schäfer, arXiv:hep-ph/0508190.
[22] K. Iida, T. Matsuura, M. Tachibana and T. Hatsuda, Phys. Rev. Lett. **93** (2004) 132001 [arXiv:hep-ph/0312363]; Phys. Rev. D **71**, 054003 (2005) [arXiv:hep-ph/0411356].
[23] K. Fukushima, C. Kouvaris and K. Rajagopal, Phys. Rev. D **71**, 034002 (2005) [arXiv:hep-ph/0408322].
[24] H. Abuki, M. Kitazawa and T. Kunihiro, Phys. Lett. B **615**, 102 (2005) [arXiv:hep-ph/0412382].
[25] S. B. Rüster, I. A. Shovkovy and D. H. Rischke, Nucl. Phys. A **743**, 127 (2004) [arXiv:hep-ph/0405170].
[26] G. Sarma, Phys. Chem. Solid **24**, 1029 (1963).
[27] H. Abuki, Master thesis submitted to Kyoto University (2000).
[28] M. Kitazawa, T. Koide, T. Kunihiro and Y. Nemoto, Prog. Theor. Phys. **108** (2002) 929 [arXiv:hep-ph/0207255].
[29] S. B. Rüster, V. Werth, M. Buballa, I. A. Shovkovy and D. H. Rischke, Phys. Rev. D **72** (2005) 034004 [arXiv:hep-ph/0503184].
[30] D. Blaschke, S. Fredriksson, H. Grigorian, A. M. Oztas and F. Sandin, Phys. Rev. D **72**, 065020 (2005) [arXiv:hep-ph/0503194].
[31] S. B. Rüster, V. Werth, M. Buballa, I. A. Shovkovy and D. H. Rischke, arXiv:hep-ph/0509073.
[32] M. Buballa and I. A. Shovkovy, Phys. Rev. D **72**, 097501 (2005) [arXiv:hep-ph/0508197].
[33] A. W. Steiner, S. Reddy and M. Prakash, Phys. Rev. D **66** (2002) 094007 [arXiv:hep-ph/0205201].
[34] M. Buballa and M. Oertel, Nucl. Phys. A **703** (2002) 770 [arXiv:hep-ph/0109095].
[35] M. Buballa, Phys. Rept. **407** (2005) 205 [arXiv:hep-ph/0402234].
[36] A. Ali Khan *et al.* [CP-PACS Collaboration], Phys. Rev. D **65** (2002) 054505 [Erratum-ibid. D **67** (2003) 059901] [arXiv:hep-lat/0105015].
[37] T. Hatsuda and T. Kunihiro, Phys. Rept. **247** (1994) 221 [arXiv:hep-ph/9401310].
[38] D. B. Kaplan and A. E. Nelson, Phys. Lett. B **175** (1986) 57.
[39] P. F. Bedaque and T. Schäfer, Nucl. Phys. A **697** (2002)

802 [arXiv:hep-ph/0105150]; D. B. Kaplan and S. Reddy, Phys. Rev. D **65**, 054042 (2002) [arXiv:hep-ph/0107265].

[40] I. Shovkovy and M. Huang, Phys. Lett. B **564**, 205 (2003) [arXiv:hep-ph/0302142]; M. Huang and I. Shovkovy, Nucl. Phys. A **729**, 835 (2003) [arXiv:hep-ph/0307273].

[41] Y. Nishida and H. Abuki, Phys. Rev. D **72**, 096004 (2005) [arXiv:hep-ph/0504083].

[42] K. Fukushima, arXiv:hep-ph/0510299.

[43] D. T. Son, Phys. Rev. D **59**, 094019 (1999) [arXiv:hep-ph/9812287].

[44] T. Schäfer and F. Wilczek, Phys. Rev. D **60**, 114033 (1999) [arXiv:hep-ph/9906512]; W. E. Brown, J. T. Liu and H. c. Ren, Phys. Rev. D **61**, 114012 (2000) [arXiv:hep-ph/9908248]; Phys. Rev. D **62**, 054016 (2000) [arXiv:hep-ph/9912409].

[45] K. Rajagopal and E. Shuster, Phys. Rev. D **62** (2000) 085007 [arXiv:hep-ph/0004074].

[46] H. Abuki, T. Hatsuda and K. Itakura, Phys. Rev. D **65**, 074014 (2002) [arXiv:hep-ph/0109013].

[47] T. Kunihiro and T. Hatsuda, Phys. Lett. B **206**, 385 (1988) [Erratum-ibid. **210**, 278 (1988)];

[48] V. Bernard, R. L. Jaffe and U. G. Meissner, Nucl. Phys. B **308**, 753 (1988).

[49] A. Kryjevski and T. Schäfer, Phys. Lett. B **606**, 52 (2005) [arXiv:hep-ph/0407329]; A. Kryjevski and D. Yamada, Phys. Rev. D **71**, 014011 (2005) [arXiv:hep-ph/0407350].

[50] M. Buballa, Phys. Lett. B **609**, 57 (2005) [arXiv:hep-ph/0410397]; M. M. Forbes, arXiv:hep-ph/0411001.

[51] L. y. He, M. Jin and P. f. Zhuang, arXiv:hep-ph/0504148; D. Ebert, K. G. Klimenko and V. L. Yudichev, Phys. Rev. D **72**, 056007 (2005) [arXiv:hep-ph/0504218].

[52] F. Neumann, M. Buballa and M. Oertel, Nucl. Phys. A **714** (2003) 481 [arXiv:hep-ph/0210078].

[53] I. Shovkovy, M. Hanuske and M. Huang, Phys. Rev. D **67**, 103004 (2003) [arXiv:hep-ph/0303027].

[54] P. F. Bedaque, H. Caldas and G. Rupak, Phys. Rev. Lett. **91**, 247002 (2003) [arXiv:cond-mat/0306694].

[55] M. G. Alford, J. A. Bowers and K. Rajagopal, Phys. Rev. D **63** (2001) 074016 [arXiv:hep-ph/0008208]; For a review, see R. Casalbuoni and G. Nardulli, Rev. Mod. Phys. **76** (2004) 263 [arXiv:hep-ph/0305069], and references therein.

[56] A. Nakamura and T. Saito, Prog. Theor. Phys. **112**, 183 (2004) [arXiv:hep-lat/0406038].

[57] K. Iida and G. Baym, Phys. Rev. D **66**, 014015 (2002) [arXiv:hep-ph/0204124].

[58] One may think it somewhat surprising that the strange quark mass jumps downwards going from 2SC to g2SC, which seemingly contradicts the discussion that plenty of strange quarks prefer the 2SC phase. However this is not the case as can be seen from FIG. 7. In fact, the Fermi momentum squared for sb quark is given by $p_{F_{sb}}^2 = (\mu + \mu_e/3 - 2\mu_s/3)^2 - M_s^2$. When one goes from the 2SC side to the g2SC side, M_s certainly drops a little, but $\mu_e(\sim 2\Delta_3)$ also drops at the transition point. The latter effect on the $p_{F_{sb}}$ wins over the former effect so that the strange quark density jumps downwards. Accordingly, the dynamical chiral condensation energy due to $\langle \bar{s}s \rangle$ gets slightly lost in the g2SC side. This energy loss is compensated by the reduction of the kinematical energy cost due to the stress arising from pinning the u - and d -Fermi momenta in the $SU(2)_{\text{color}}$ sector at equal level in the 2SC side (see the decrease of μ_e from 2SC to g2SC). As a consequence of these competing dynamical and kinematical ingredients, $\Omega_{\text{2SC}} = \Omega_{\text{g2SC}}$ holds at $\mu = 494.8$ MeV, i.e., the 2SC/g2SC transition point.

[59] It is not strange that we have arrived at the same expression for the Ginzburg-Landau potential as that in [22] although we have derived it from the diquark NJL model with the contact two fermion interaction. This is simply because the non-locality of the gluon-mediated attraction is incorporated into the Ginzburg-Landau potential only through T_{c0} and the gap function $\Delta_0(p)$ with p being the momentum of quasi-quarks in [22].